Dietary tryptophan catabolite released by intratumoral Lactobacillus reuteri facilitates αPD-L1 therapy

Mackenzie Bender
University of Pittsburgh
Alex McPherson
University of Pittsburgh
Catherine Phelps
University of Pittsburgh
Mohit Rana
University of Pittsburgh
Surya Pandey
University of Pittsburgh
Jake Shapira
University of Pittsburgh
Angela Gocher
Department of Immunology, University of Pittsburgh School of Medicine
Steven Mullett
University of Pittsburgh
Stacy Wendell
University of Pittsburgh
Diwakar Davar
University of Pittsburgh, UPMC Hillman Cancer Center
Reinhard Hinterleitner
University of Pittsburgh
Dario Vignali
University of Pittsburgh https://orcid.org/0000-0002-2771-5992
Alok Joglekar
University of Pittsburgh
Hassane Zarour
University of Pittsburgh https://orcid.org/0000-0003-2525-2688
Marlies Meisel (Marlies@pitt.edu)
University of Pittsburgh https://orcid.org/0000-0001-5156-8067

Biological Sciences - Article

Keywords:

Posted Date: May 18th, 2022

DOI: https://doi.org/10.21203/rs.3.rs-1633600/v1

Abstract

The gut microbiome has been identified as a critical factor influencing cancer patient responses to immune checkpoint inhibitor (ICI) therapy; however, the underlying mechanisms of how gut microbes modulate ICI therapy efficacy remain enigmatic. Here, we show that gut-commensal Lactobacillus reuteri (L. reuteri) translocates to melanoma tumors where it mediates antitumor interferon-γ-producing CD8 T cell (Tc1 cell) immunity and facilitates ICI therapy via its released aryl hydrocarbon receptor (AhR) ligand, indole-3-aldehyde (I3A). This dietary tryptophan (Trp) catabolite is necessary and sufficient for antitumor immunity, and AhR signaling within CD8 T cells is required for L. reuteri to suppress melanoma growth. Further, a Trp-enriched diet potentiated L. reuteri- and ICI-induced antitumor immunity. Finally, we uncovered a role of I3A in promoting ICI therapy responses and survival in advanced melanoma patients. Collectively, our findings elucidate a novel crosstalk within the tumor microenvironment between the microbial metabolite I3A and CD8 T cells that facilitates ICI therapy efficacy, paving the way for dietary- and probiotic-based cancer therapeutics.

Main Text

Reinvigorating antitumor immunity by immune checkpoint inhibitor (ICI) treatment is a core component of cancer therapy that has shown unprecedented efficacy in a fraction of cancer patients suffering from renal cell carcinoma, non-small cell lung cancer, or advanced melanoma (*1-4*). While the blockade of inhibitory T cell receptors, such as programmed cell death-1 (PD-1) or its ligand PD-L1, unleashes antitumor T cell immune responses against cancer (*5, 6*) and displays potent clinical efficacy, only 40% of melanoma patients respond to treatment (*7*). Therefore, approaches that further potentiate antitumor T cell immunity are needed to boost ICI therapy efficacy in melanoma. Primary resistance to ICI therapy treatment in melanoma patients has been associated with endogenous factors, such as oncogenic signaling pathways in tumor cells (*8*), poor tumor antigen presentation (*9*), and low tumor mutational burden (*10*), as well as exogenous factors- including an unfavorable gut microbiome composition (*11*). The gut microbiome has been identified as a critical tumor-extrinsic factor that modulates responsiveness to ICI therapy, as oral administration of specific commensal bacteria or fecal microbial transplantation (FMT) of ICI-responder feces were found to potentiate ICI therapy efficacy in preclinical studies (*12-16*). Recently, results of clinical trials revealed that FMT of ICI responder patient feces overcomes ICI therapy resistance in ICI non-responder melanoma patients (*17, 18*). Despite major advances in the field, the underlying mechanisms of how host-microbiota interactions shape systemic tumor immunity and affect ICI therapy efficacy in gut-distal tumors, such as melanoma, remain poorly understood. In this study we used a preclinical melanoma model to identify gut bacteria, found to be expanded in ICI responder melanoma patients, capable of suppressing tumor growth, and further, explored the host-microbial crosstalk that enables the most potent tumor-suppressing strain to increase ICI therapy efficacy. Moreover, we interrogated the clinical relevance of our preclinical findings in a cohort of advanced melanoma patients that either responded or failed to respond to ICI therapy.

L. reuteri induces antitumor immunity and promotes ICI therapy in preclinical melanoma

We used a preclinical melanoma model to test the antitumor potential of four commensal bacterial species representative of the bacterial taxa *Bifidobacteriaceae*, *Enterobacteriaceae*, and *Lactobacilliaceae*, all found to be overabundant in ICI responder melanoma patient feces (*15, 17, 19-22*). The growing interest of probiotic supplementation in cancer patients prompted us to select *Bifidobacterium longum* (*B. longum, Bifidobacteriaceae*), *Lactobacillus reuteri* (*L. reuteri, Lactobacilliaceae*), *Lactobacillus johnsonii* (*L. johnsonii, Lactobacilliaceae*) and *Escherichia coli* (*E. coli, Enterobacteriaceae*) as representative species of the given taxa due to their frequent therapeutic use as commercially-available probiotics (*15*). Given antibiotic (ABX) treatment negatively impacts on the response to cancer immunotherapy (*13, 14, 16, 23*) and probiotic therapeutics are typically supplemented daily (*24*), we chose a treatment regimen where non-ABX treated specific pathogen–free (SPF) mice were orally gavaged daily with the selected bacterial taxa. We found that independent daily oral administration of *B. longum, E. coli*, or *L. reuteri* starting one day post B16-F0 subcutaneous tumor cell engraftment efficiently restrained melanoma growth (Fig. 1a, b) and increased survival (Fig. 1c) in SPF C57BL/6 wild type (WT) mice from The Jackson Laboratory relative to vehicle control treated mice. Interestingly, *L. johnsonii* failed to mediate tumor growth suppression, indicating that the ability of commensals to suppress tumor growth in our model is species specific. The tumor suppressive effect of *B. longum* is in line with findings by others (*12*). Intriguingly, *L. reuteri* induced the most potent tumor suppression relative to vehicle control, and further showed significant tumor suppression relative to both *B. longum* and *E. coli*. Hypothesizing that the underlying mechanisms by which these phylogenetically different probiotic bacteria promote tumor suppression may be distinct, we set out to specifically explore the mechanism of how *L. reuteri*, the gut commensal and dietary probiotic with the most potent tumor suppressive ability in our model, restrains melanoma outgrowth.

Implying both prophylactic and therapeutic *L. reuteri* treatment is effective in restraining tumor growth, we found that oral administration of *L. reuteri* was capable of significantly suppressing tumor outgrowth and prolonging survival in mice post tumor establishment (approximately 150 mm^3) (Extended Data Fig. 1a, b). We found daily oral administration of *L. reuteri* led to a significant increase in the relative abundance of *L. reuteri* in the small intestine, but not the cecum or colon, compared to vehicle control mice (Extended Data Fig. 1c), which is in line with the finding that *L. reuteri* was found to colonize the small intestine of a healthy human cohort following probiotic supplementation with *L. reuteri* (*25*). Given the possibility that *L. reuteri* treatment-induced gut dysbiosis plays a role in *L. reuteri*-mediated tumor suppression, we orally gavaged germ free melanoma-bearing mice with *L. reuteri* or vehicle control, and found *L. reuteri* to be capable of suppressing melanoma growth independent of a pre-established microbiome (Fig. 1d).

In order to better understand how *L. reuteri* suppresses tumor growth, we were prompted to assess the systemic immunoregulatory consequences of *L. reuteri* administration. Upon assessing the immune response of melanoma-bearing mice at day 17 post tumor cell engraftment via flow cytometry (Extended Data Fig. 2a, b), we found that *L. reuteri* treatment skews the tumor microenvironment (TME) towards an antitumorigenic, immunostimulatory environment, characterized by an expansion of interferon-g (IFNg) producing CD4 Th1 and CD8 Tc1 cells (Fig. 1e, f) that undergo active proliferation, evidenced by their

Ki67 expression (Extended Data Fig. 2c, d). Furthermore, tumor-infiltrating Th1 and Tc1 cells of *L. reuteri* treated tumor-bearing mice demonstrated a significant increase in cytotoxic Granzyme B (GzmB) production relative to PBS treated mice (Extended Data Fig. 2e, f). Interestingly, even though the frequency of Foxp3^{+} regulatory T cells (Tregs) within the TME remained largely unaffected in *L. reuteri* treated tumor-bearers relative to PBS treated mice (Extended Data Fig. 2g), *L. reuteri* treatment led to a significant expansion of IFNg^{+} Treg cells within the TME (Extended Data Fig. 2h). *L. reuteri* treatment was insufficient to promote type 1 effector T cell function within the spleen, indicating that *L. reuteri* mediates antitumor T cell immune responses selectively within the TME (Extended Data Fig. 2i-n). In line with the finding that adaptive immunity is required for *L. reuteri*-mediated tumor suppression (Extended Data Fig. 3a), *L. reuteri* failed to majorly impact on innate immune responses in the TME (Extended Data Fig. 3b-d). *In vivo* depletion studies revealed that CD8, but not CD4, T cells are required for *L. reuteri*-mediated tumor suppression (Extended Data Fig. 3e), thus, to fully characterize the impact of *L. reuteri* on tumor-infiltrating CD8 T cells we performed single-cell RNA-sequencing analysis of CD8 T cells derived from the TME. Unsupervised clustering identified 13 distinct CD8 T cell clusters, including naïve (clusters 0 and 1), memory (clusters 3, 8, and 12) and proliferating, cytotoxic, pre-exhausted/exhausted effector (predominately clusters 4 and 6) subsets (Extended Data Fig. 4a, b, Extended Data Table 1, Supplementary Information Table 1). Trajectory and differential gene expression analysis revealed that *L. reuteri* treatment skews the cell distribution towards a cytotoxic effector profile, characterized by high levels of *Ifng*, *Prf1* (encodes perforin), *Gzmb*, *Nkg7* (encodes natural killer cell granule protein), and *Tbx21* (encodes T-bet transcription factor 21 (*Tbet*)) (Fig. 1g, Extended Data Fig. 4c to e, Extended Data Table 1, Supplementary Information Table 1). The finding that *L. reuteri* treatment led to a significant enrichment in the expression of inhibitory T cell receptors *Tigit* (encodes T cell immunoreceptor with Ig and ITIM domains), *Pdcd1* (encodes PD1) and *Lag3* (encodes Lymphocyte Activating 3) in tumor-infiltrating CD8 T cells (Fig. 1g), in concert with the observation that human melanoma-infiltrating PD1-expressing CD8 T cells are positive predictive biomarkers for aPD1 therapy (*26*), prompted us to assess the potential role of *L. reuteri* in potentiating ICI therapy efficacy (Extended Data Fig. 4f). Indeed, mice who received combinatorial treatment with both *L. reuteri* and aPD-L1 showed significantly improved tumor control (Fig. 1h, i), and the most pronounced antitumor Tc1 cell immunity within the TME (Extended Data Fig. 4g), relative to mice that received aPD-L1 or *L. reuteri* alone, confirming the ability of *L. reuteri* to potentiate ICI therapy-mediated tumor suppression. The finding that *L. reuteri* induces an expansion of Tc1 cells, in conjunction with the key role of Tc1 cells in promoting ICI therapy efficacy (*5, 6*), prompted us to test whether *L. reuteri*-mediated antitumor immunity is dependent on IFNg production by CD8 T cells. Indeed, we found that *L. reuteri* failed to suppress tumor growth (Fig. 1j) or increase survival (Fig. 1k) in *Ifng*$^{L/L}$ *E8I Cre*$^{+}$ mice, unlike Cre^{-} littermate controls, demonstrating that production of IFNg by CD8 T cells is required for *L. reuteri*-mediated tumor suppression. Collectively, these results demonstrate that *L. reuteri* is effective in enhancing both spontaneous and ICI therapy-mediated antitumor immunity in a Tc1 cell-dependent manner.

Presence of *L. reuteri* within the tumor is necessary and sufficient to mediate antitumor effects in melanoma

Accumulating evidence suggests the presence of a tumor microbiome in gut-distal cancers, including melanoma (*27-30*), and live bacteria have been recovered from breast (*29, 31*) and pancreatic tumor cultures (*27, 28*). To this end, we tested whether viable *L. reuteri* was present within melanoma tumors. Indeed, we detected viable *L. reuteri* in all tumors of mice orally administered *L. reuteri* by culturing tumor homogenate in *Lactobacilli*-selective medium (Fig. 2a, b, Extended Data Fig. 5a, b). While we detected *L. johnsonii* in one tumor of a PBS treated mouse, we failed to detect *L. reuteri* in PBS treated mice (Extended Data Fig. 5b). To better understand the underlying mechanism of how *L. reuteri* translocates to gut-distal melanoma tumors, we assessed whether daily oral administration of *L. reuteri* impairs intestinal barrier integrity in tumor bearing mice, leading to an increased ability of commensals to escape the gut. However, we found that *L. reuteri* treatment failed to elevate intestinal permeability relative to vehicle control treated tumor bearers (Extended Data Fig. 5c). Accordingly, jejunal and colonic gene expression of key tight junction genes *tight junction zonula occludens-1* (*Zo-1*), *tight junction protein 2* (*Tjp2*), *occludin* (*Ocln*) and *desmoplakin* (*Dsp*) remained grossly unaffected (Extended Data Fig. 5d). Indicating the ability to translocate to gut-distal tumors is not specific to *L. reuteri*, we detected viable *E. coli* within melanoma tumors of mice orally administered *E. coli* in contrast to vehicle control treated mice (Extended Data Fig. 5e). Similar to others (*12*), we failed to detect *B. longum* within melanoma tumors of mice orally administered *B. longum*, suggesting either not all commensals can translocate to, or persist within, gut-distal melanoma (Extended Data Fig. 5f). To test whether *L. reuteri* can colonize and persist within melanoma tumors, we injected a single dose of 2×10^7 colony forming units (CFU) *L. reuteri* intratumorally and found that despite a reduction in abundance over time, viable *L. reuteri* could be cultured from *L. reuteri*-injected tumors up to 12 days post injection (Fig. 2c), suggesting the TME provides a sustainable niche for *L. reuteri*.

Demonstrating that the presence of viable *L. reuteri* within the tumor is sufficient to promote antitumor immunity, intratumoral injection of *L. reuteri*, but not vehicle control, into established tumors (averaging 150 mm^3 in size) efficiently suppressed tumor outgrowth (Fig. 2d), significantly enhanced the induction of Tc1 cell frequencies within the tumor (Fig. 2e), and significantly prolonged survival (Fig. 2f). Given these observations and that *L. reuteri* is naturally present within the intestinal tract of WT C57BL/6 mice (*32*), we assessed whether intratumoral *L. reuteri* is required for *L. reuteri*-mediated tumor suppression. To do so, we used the antibiotics ampicillin (AMP) and vancomycin (VAN), found to effectively (*33-35*) or ineffectively deplete *L. reuteri* (*34*), respectively, which we confirmed *in vitro* (Extended Data Fig. 5g). Once tumors reached approximately 200 mm^3 in size, mice received daily oral gavages of *L. reuteri* or PBS in combination with intratumoral injections of VAN or AMP every other day (Extended Data Fig. 5h). Interestingly, in stark contrast to mice who received intratumoral injections of VAN, mice who received intratumoral injections of AMP failed to show significant tumor suppression (Fig. 2g) or benefit on survival (Fig. 2h) when treated with *L. reuteri*. Notably, intratumoral AMP treatment led to a ~3-log decrease of viable *L. reuteri* within tumors when compared to VAN injected tumors of *L. reuteri* treated mice (Fig. 2i), but failed to majorly affect the relative abundance of *L. reuteri* within the small intestine or overall fecal bacterial load (Extended Data Fig. 5i, j). Taken together, these data suggest that intratumoral

L. reuteri is sufficient and required to promote antitumor Tc1 cell immunity, suppress tumor outgrowth, and increase survival in preclinical melanoma.

L. reuteri released tryptophan catabolite indole-3-aldehyde (I3A) is required and sufficient to promote antitumor immunity and restrain tumor growth

We next sought to determine the mechanistic basis of how *L. reuteri* drives tumor suppression. To this end, we first interrogated whether *L. reuteri*-mediated tumor suppression is melanoma-model specific and whether oral administration of *L. reuteri* is effective in restraining tumor growth in other cancer models. Interestingly, *L. reuteri* treatment of mice bearing either subcutaneous ICI-resistant Yumm1.7 melanoma (*36*) or MC38 adenocarcinoma led to significantly delayed tumor outgrowth (Extended Data Fig. 6a, b). Suggesting that translocation to, and persistence within, gut-distal tumors of *L. reuteri* is not limited to B16 melanoma, viable *L. reuteri* were detected in both Yumm1.7 as well as MC38 tumors (Extended Data Fig. 6a, b). Next, we set out to test whether physical components of *L. reuteri* are sufficient to mitigate B16 melanoma outgrowth. In stark contrast to mice treated with viable *L. reuteri*, neither oral administration nor direct intratumoral injection of heat-killed *L. reuteri* was sufficient to suppress tumor growth or prolong survival (Extended Data Fig. 6c-f). These observations pointed towards an *L. reuteri*-induced antitumor mechanism that occurs in a tumor- and *L. reuteri*-antigen-independent fashion, likely dependent on the metabolic activity of *L. reuteri*.

L. reuteri has been shown to release several immunomodulatory metabolites including the indole-derivative indole-3-aldehyde (I3A), which has been shown to have T cell immunomodulatory properties through activation of the aryl hydrocarbon receptor (AhR), an ubiquitously expressed transcription factor (*37*). To this end, we set out to interrogate whether I3A released by *L. reuteri* plays a key role in *L. reuteri*-induced Tc1 cell-mediated antitumor immunity by treating mice with a genetically modified strain of *L. reuteri* that lacks the gene for the aromatic amino acid aminotransferase class I/II (*L. reuteri* DArAT), abrogating its ability to catabolize dietary tryptophan (Trp) into I3A (*37, 38*) (Extended Data Fig. 7a-c). Strikingly, we found that in stark contrast to *L. reuteri* WT, oral administration of *L. reuteri* DArAT failed to suppress tumor growth (Fig. 3a), increase survival (Fig. 3b), or trigger a potent antitumor Tc1 cell immune response within the TME (Fig. 3c) relative to vehicle control treated mice. Upon sterilely culturing tumors from mice treated with *L. reuteri* WT or DArAT, we found both viable *L. reuteri* strains to be present within tumors (Fig. 3d), indicating the lack of tumor suppression or induction of Tc1 cell immunity by *L. reuteri* DArAT was not due to a defect in its ability to translocate to the tumor. Of note, we could detect *L. reuteri* in one tumor of a PBS treated mouse, indicating that *L. reuteri* can translocate to gut-distal melanoma even in absence of probiotic supplementation (Fig. 3d). Through sub-culturing viable *L. reuteri* recovered from the tumors of *L. reuteri* WT or DArAT treated mice in Trp-enriched media, we confirmed that translocated *L. reuteri* WT, but not *L. reuteri* DArAT, maintained the ability to catabolize Trp into AhR ligands *ex vivo* using an AhR reporter cell line (Extended Data Fig. 7d). This coincided with a significant increase in AhR activity and abundance of I3A in the tumor homogenate of *L. reuteri* WT treated mice compared to both *L. reuteri* DArAT and vehicle control treated mice (Fig. 3e, f), suggesting *L. reuteri* WT releases the AhR agonist, I3A, within the tumor. Further confirming the critical role of microbial released

I3A, *L. johnsonii*, which failed to suppress tumor growth (Fig. 1a, b), is a phylogenetically related strain to *L. reuteri* which naturally lacks the ability to produce I3A (*38*).

Upon establishing the requirement of I3A in *L. reuteri*-mediated tumor suppression, we were prompted to assess whether I3A alone is sufficient to induce antitumor Tc1 cell immunity and suppress tumor growth. Indeed, oral administration of I3A suppressed tumor growth and increased survival in a dose-dependent manner (Fig. 3g, h). Further, upon assessing tumor-infiltrating lymphocytes in I3A treated mice, we found oral administration with I3A was sufficient to significantly elevate Tc1 cell effector function in the TME relative to vehicle control treated mice (Fig. 3i). Intratumoral injections of I3A also led to significant tumor suppression and increased survival (Extended Data Fig. 7e-f) in a dose-dependent manner, indicating I3A can suppress tumor growth from directly within the TME. These findings prompted us to assess the ability of I3A to potentiate aPD-L1-mediated tumor suppression. Interestingly, combinatorial treatment with both I3A and aPD-L1 led to a significant decrease in tumor growth compared to treatment with aPD-L1 alone (Fig. 3j), and only mice who received both I3A and aPD-L1 showed a significant decrease in tumor weight relative to mice treated with vehicle and isotype control (Fig. 3k).

Taken together, our data reveal that *L. reuteri*-derived I3A is required and sufficient to promote spontaneous antitumor Tc1 cell immunity and melanoma suppression, and further, potentiates the efficacy of aPD-L1-mediated tumor suppression.

I3A mediates antitumor immunity via activation of AhR within CD8 T cells

AhR activation has been demonstrated to play a critical role in skewing CD4 T cell differentiation towards the Th17 or Treg cell linage in a ligand-dependent fashion (*39, 40*). However, the impact of microbial AhR ligands on Tc1 cell function remains undefined. To determine whether *L. reuteri* released AhR agonist I3A directly acts on CD8 T cells to promote IFNg production, we cultured splenic naïve CD8 T cells, activated with aCD3 and aCD28, with supernatant derived from *L. reuteri* WT or *L. reuteri* DArAT, which activates or fails to activate AhR, respectively (Extended Data Fig. 7g), for 72 hours. We observed that *L. reuteri* WT-derived supernatant substantially promoted IFNg production, yet supernatant of *L. reuteri* DArAT failed to induce IFNg production in CD8 T cells (Extended Data Fig. 7h), indicating that *L. reuteri* released AhR ligand I3A directly acts on CD8 T cells to promote Tc1 cell effector function. Further, to test the requirement of AhR activation within CD8 T cells in *L. reuteri*-mediated antitumor immunity *in vivo*, we generated mice with a specific deletion of AhR in CD8 T cells (*Ahr*$^{fl/fl}$ *Cd8* Cre^{+}). Strikingly, we found both *L. reuteri*- and I3A-mediated tumor suppression as well as benefit on survival to be abrogated in *Ahr*$^{fl/fl}$ *Cd8 Cre*$^{+}$ mice in contrast to *Cre*$^{-}$ littermate controls (Fig. 4a-d), revealing that *L. reuteri* released I3A-mediated tumor suppression is dependent on CD8 T cell-intrinsic AhR activation. Concordant with the inability of I3A to suppress tumor growth in *Ahr*$^{fl/fl}$ *Cd8* Cre^{+} mice, I3A treatment failed to induce a robust Tc1 cell response in *Ahr*$^{fl/fl}$ *Cd8* Cre^{+} mice (Fig. 4e), indicating that the *L. reuteri*-derived I3A-mediated antitumor response is dependent on CD8 T cell-intrinsic AhR signaling.

Taken together, these results indicate that *L. reuteri* derived I3A directly acts on CD8 T cells to promote IFNg production, consequently driving antitumor responses in preclinical melanoma.

Tryptophan-enriched diet facilitates ICI therapy efficacy

Given dietary Trp is the required substrate used by commensal taxa capable of catabolizing dietary Trp into AhR ligands such as I3A (*38*), we assessed whether dietary Trp levels affect *L. reuteri*-mediated antitumor responses in preclinical melanoma. To this end, mice were placed on diets identical in nutrient composition that differed only in amount of Trp for four weeks prior to tumor cell implantation and stayed on their respective diets for the entirety of the experiment (Extended Data Fig. 8a). While a Trp-low (0.19%) diet did not fully abrogate *L. reuteri*'s ability to suppress tumor growth, mice who received *L. reuteri* on a Trp-high (1.19%) diet showed significant tumor suppression and increased survival relative to mice who received *L. reuteri* on a Trp-low diet (Fig. 4f-h), indicating a Trp-enriched diet potentiates *L. reuteri*-mediated tumor suppression. Interestingly, we observed that a Trp-high diet alone was sufficient to restrain melanoma growth and prolong survival relative to a Trp-low diet (Fig. 4f-h). Further, we found the observed antitumor effect of both a Trp-high diet alone and combinatorial Trp-high and *L. reuteri* treatment directly correlated with increased AhR activity of tumor homogenates (Fig. 4i, j), suggesting a Trp-enriched diet promotes antitumor responses by increasing AhR activity within the TME. Given that a Trp-enriched diet is sufficient to suppress tumor growth in the absence of exogenously administered *L. reuteri*, we assessed whether a Trp-enriched diet alone could potentiate ICI therapy efficacy. Interestingly, we observed that maintaining mice on a Trp-enriched diet significantly potentiates aPD-L1 immunotherapy efficacy when compared to aPD-L1 treated mice maintained on a Trp-low diet (Fig. 4k, l).

The finding that a Trp-enriched diet is sufficient to mediate antitumor responses in the presence of a complex microbiome suggests that other Trp catabolizing bacteria potentially contribute to antitumor immunity in our model. In line with this hypothesis, the ability to catabolize dietary Trp into AhR ligands is not limited to *L. reuteri* but extends to other commensal gut bacteria, including *E. coli* ((*41*) and Extended Data Fig. 8b), which we found to potently suppress melanoma outgrowth in our model (Fig. 1a, b). To interrogate whether *E. coli* restrains tumor growth via a mechanism similar to *L. reuteri*, we first addressed the requirement of metabolic activity in *E. coli*-mediated tumor suppression by intratumorally injecting melanoma-bearing mice with either viable or heat-killed *E. coli*. Interestingly, while heat-killed *E. coli* suppressed tumor growth relative to vehicle control, viable *E. coli* displayed significant tumor suppression relative to heat-killed *E. coli*, indicating the metabolic activity of *E. coli* contributes significantly to *E. coli*-mediated antitumor effects (Extended Data Fig. 8c). Interestingly, upon assessment of the TME of mice orally administered viable *E. coli*, we found *E. coli* treatment led to both an expansion of Tc1 cells and an increase in AhR activity within the TME (Extended Data Fig. 8d, e). Further, increased AhR activity within the TME of *E. coli* treated mice directly correlated with antitumor Tc1 cell immunity (Extended Data Fig. 8f), suggesting that, in part, *E. coli* promotes antitumor responses by increasing AhR activity within the TME.

Taken together, we found that a Trp-enriched diet potentiates the antitumor effect of *L. reuteri*, and in the presence of a complex-microbiota, an enriched Trp diet enhances ICI therapy efficacy.

Evidence for a role of I3A in promoting ICI therapy responses and survival in advanced melanoma patients

To directly investigate a potential role of I3A in influencing ICI therapy efficacy in human melanoma, we performed targeted mass spectrometry to determine baseline I3A sera levels of advanced, stage IV melanoma patients (n = 42) that either responded (n = 19) or remained resistant (n = 23) to combinatorial IFNa and aPD1 immunotherapy, based on RECIST v1.1 criteria (33). Concordant with our novel findings in preclinical melanoma, the abundance of exogenous I3A in sera of advanced melanoma patients at baseline was significantly elevated in ICI responders when compared to ICI non-responders (Fig. 5a). To further interrogate the clinical significance and prognostic relevance of this finding, we assessed the impact of pre-treatment, systemic I3A levels on progression-free survival (PFS) and overall survival of the cohort. By stratifying patients by high (> 70th percentile) and low (< 30th percentile) serum I3A concentrations, we identified that patients that displayed high systemic I3A at baseline exhibited significantly prolonged PFS and overall survival in contrast to patients with low I3A levels at baseline (Fig. 5b, c). As serum levels of endogenous AhR ligands, specifically kynurenine (Kyn), have been found to be increased in advanced melanoma patients and have been associated with poor prognosis (34, 35), we were prompted to assess serum levels of Kyn in the same cohort of advanced melanoma patients. In contrast to I3A, ICI responders and non-responders displayed a similar systemic abundance of Kyn at baseline (Fig. 5d), and further, no statistical differences in either PFS or overall survival were found when patients were stratified by high (> 70th percentile) and low (< 30th percentile) Kyn serum concentrations (Fig. 5e, f). These findings prompted us to assess the impact of the endogenous AhR ligand Kyn in our model. In line with the finding that Kyn serum concentrations at baseline had no impact on PFS or overall survival in patients, only intratumoral injections of I3A, but not Kyn, suppressed tumor growth in melanoma-bearing mice (Fig. 5g), indicating tumor suppression via activation of the AhR is ligand dependent in preclinical melanoma.

Taken together, these findings imply that the microbial AhR ligand I3A plays a role in promoting ICI therapy responses in melanoma patients, contributing to prolonged PFS and overall survival.

Discussion

Collectively, our findings elucidate a critical microbial-host crosstalk within the TME that potently enhances spontaneous antitumor immunity and facilitates ICI therapy efficacy in preclinical melanoma. More specifically, our data suggest that *L. reuteri* translocates to, colonizes, and persists within melanoma tumors where it locally promotes antitumor CD8 T cell immunity via released AhR agonist and dietary Trp catabolite, I3A. We uncovered that *L. reuteri*-derived I3A directly acts through CD8 T cell-specific AhR signaling to promote antitumor IFNg producing CD8 T cells and found that I3A is sufficient and required to facilitate ICI therapy in melanoma. Additionally, we revealed that a Trp-enriched diet is

sufficient to facilitate ICI therapy and that the antitumor effects of a Trp-enriched diet directly correlate with an increase in AhR activity within the TME. Finally, we uncovered a role of I3A in promoting ICI therapy responses and survival in advanced melanoma patients (Extended Data Fig. 9).

Our findings that *E. coli*, which produces AhR ligands via catabolism of Trp, induce Tc1 cell expansion within the TME, and its antitumor effects directly correlate with increased TME AhR activity, suggest the mechanism by which *L. reuteri* induces antitumor immunity via activation of the AhR within CD8 T cells may not be specific to *L. reuteri*, but rather extends to AhR-ligand releasing bacteria. Thus, future studies will be needed to address the extent to which this mechanism is conserved among Trp-derived AhR ligand releasing commensals.

The mechanism by which a Trp-enriched diet potentiates ICI therapy efficacy remains to be fully addressed. The hypothesis that a Trp-enriched diet leads to an expansion of AhR ligand-producing commensals, leading to an induction of antitumor immunity through increased AhR activation within CD8 T cells will be tested in future studies. Additional mechanistic studies to interrogate the molecular mechanism of how the microbial AhR agonist I3A promotes a type 1 immune program in CD8 T cells will also be of interest. In addition, the mechanism of how gut commensal bacteria such as *L. reuteri* translocate to gut-distal cancers, including melanoma, remains to be addressed.

Our findings that the endogenous AhR ligand Kyn was similarly abundant between ICI melanoma responders and non-responders (Fig. 5D) and that patients with high systemic Kyn did not display a significant difference in PFS or overall survival compared to patients with low Kyn (Fig. 5E to F) is in line with the finding that despite Kyn having been shown to have pro-cancerogenic properties in a model of pre-clinical melanoma (*42*), clinical trials to block endogenous AhR signaling failed to provide protection (*43*). These findings, in concert with our work, suggest that the role of AhR activation in tumor progression is ligand-specific, and future studies will be needed to distinguish the roles of exogenous versus endogenous ligand activation of the AhR within CD8 T cells in influencing tumor immunity in melanoma.

While recently microbial Ahr ligands have been found to display pro-tumorigenic effects in a murine pancreatic cancer model via activation of the AhR in myeloid cells (*44*), the impact of the AhR in cancer has been shown to be context, ligand, and tumor dependent, highlighting the importance of studying the role of microbial-derived activation of the AhR in various cancer models.

A recent observational study revealed that dietary fiber and probiotic intake modulate ICI therapy efficacy in human melanoma (*20*). In line with this, our work provides a mechanism of how the probiotic *L. reuteri*, by utilizing dietary Trp, invigorates tumor-infiltrating CD8 T cell effector function and thereby mediates spontaneous antitumor immunity and facilitates ICI therapy efficacy in preclinical melanoma.

Our study has translational potential given that (i) *Lactobacilli* are found to be enriched in ICI responder melanoma patients when compared to non-responders (*15, 17, 19*), (ii) *L. reuteri* is one of the most widely used probiotic that is naturally present in the human intestine (*45*), (iii) our study used a human-isolated

L. reuteri strain, and (iv) our study uncovered a role of I3A in promoting ICI therapy responses in melanoma patients. The potential role of I3A as a biomarker for ICI sensitivity in melanoma requires further investigation in human melanoma patients. In addition, future studies will address the role of I3A in patients suffering from other ICI-resistant cancer types.

Our study will motivate a new line of investigations and provides a rational mechanistic basis to design novel dietary and probiotic combinatorial therapeutic strategies to determine the clinical antitumor effect of microbial AhR ligands, such as I3A, in ICI-resistant cancer patients.

References

1. F. S. Hodi *et al.*, Improved survival with ipilimumab in patients with metastatic melanoma. *N Engl J Med* **363**, 711-723 (2010).

2. C. Robert *et al.*, Ipilimumab plus dacarbazine for previously untreated metastatic melanoma. *N Engl J Med* **364**, 2517-2526 (2011).

3. S. L. Topalian *et al.*, Safety, activity, and immune correlates of anti-PD-1 antibody in cancer. *N Engl J Med* **366**, 2443-2454 (2012).

4. O. Hamid *et al.*, Safety and tumor responses with lambrolizumab (anti-PD-1) in melanoma. *N Engl J Med* **369**, 134-144 (2013).

5. B. C. Miller *et al.*, Subsets of exhausted CD8(+) T cells differentially mediate tumor control and respond to checkpoint blockade. *Nat Immunol* **20**, 326-336 (2019).

6. M. Sade-Feldman *et al.*, Defining T Cell States Associated with Response to Checkpoint Immunotherapy in Melanoma. *Cell* **175**, 998-1013 e1020 (2018).

7. P. Sharma, J. P. Allison, The future of immune checkpoint therapy. *Science* **348**, 56-61 (2015).

8. S. Spranger, R. Bao, T. F. Gajewski, Melanoma-intrinsic beta-catenin signalling prevents anti-tumour immunity. *Nature* **523**, 231-235 (2015).

9. M. Luksza *et al.*, A neoantigen fitness model predicts tumour response to checkpoint blockade immunotherapy. *Nature* **551**, 517-520 (2017).

10. A. Snyder *et al.*, Genetic basis for clinical response to CTLA-4 blockade in melanoma. *N Engl J Med* **371**, 2189-2199 (2014).

11. J. M. Pitt *et al.*, Resistance Mechanisms to Immune-Checkpoint Blockade in Cancer: Tumor-Intrinsic and -Extrinsic Factors. *Immunity* **44**, 1255-1269 (2016).

12. A. Sivan *et al.*, Commensal Bifidobacterium promotes antitumor immunity and facilitates anti-PD-L1 efficacy. *Science* **350**, 1084-1089 (2015).

13. M. Vetizou *et al.*, Anticancer immunotherapy by CTLA-4 blockade relies on the gut microbiota. *Science* **350**, 1079-1084 (2015).

14. B. Routy *et al.*, Gut microbiome influences efficacy of PD-1-based immunotherapy against epithelial tumors. *Science* **359**, 91-97 (2018).

15. V. Matson *et al.*, The commensal microbiome is associated with anti-PD-1 efficacy in metastatic melanoma patients. *Science* **359**, 104-108 (2018).

16. V. Gopalakrishnan *et al.*, Gut microbiome modulates response to anti-PD-1 immunotherapy in melanoma patients. *Science* **359**, 97-103 (2018).

17. E. N. Baruch *et al.*, Fecal microbiota transplant promotes response in immunotherapy-refractory melanoma patients. *Science* **371**, 602-609 (2021).

18. D. Davar *et al.*, Fecal microbiota transplant overcomes resistance to anti-PD-1 therapy in melanoma patients. *Science* **371**, 595-602 (2021).

19. K. A. Lee *et al.*, Cross-cohort gut microbiome associations with immune checkpoint inhibitor response in advanced melanoma. *Nat Med* **28**, 535-544 (2022).

20. C. N. Spencer *et al.*, Dietary fiber and probiotics influence the gut microbiome and melanoma immunotherapy response. *Science* **374**, 1632-1640 (2021).

21. J. A. McCulloch *et al.*, Intestinal microbiota signatures of clinical response and immune-related adverse events in melanoma patients treated with anti-PD-1. *Nat Med* **28**, 545-556 (2022).

22. A. Limeta, B. Ji, M. Levin, F. Gatto, J. Nielsen, Meta-analysis of the gut microbiota in predicting response to cancer immunotherapy in metastatic melanoma. *JCI Insight* **5**, (2020).

23. A. Elkrief, L. Derosa, G. Kroemer, L. Zitvogel, B. Routy, The negative impact of antibiotics on outcomes in cancer patients treated with immunotherapy: a new independent prognostic factor? *Ann Oncol* **30**, 1572-1579 (2019).

24. J. Suez, N. Zmora, E. Segal, E. Elinav, The pros, cons, and many unknowns of probiotics. *Nat Med* **25**, 716-729 (2019).

25. N. Valeur, P. Engel, N. Carbajal, E. Connolly, K. Ladefoged, Colonization and immunomodulation by Lactobacillus reuteri ATCC 55730 in the human gastrointestinal tract. *Appl Environ Microbiol* **70**, 1176-1181 (2004).

26. P. C. Tumeh *et al.*, PD-1 blockade induces responses by inhibiting adaptive immune resistance. *Nature* **515**, 568-571 (2014).

27. L. T. Geller *et al.*, Potential role of intratumor bacteria in mediating tumor resistance to the chemotherapeutic drug gemcitabine. *Science* **357**, 1156-1160 (2017).

28. E. Riquelme *et al.*, Tumor Microbiome Diversity and Composition Influence Pancreatic Cancer Outcomes. *Cell* **178**, 795-806 (2019).

29. D. Nejman *et al.*, The human tumor microbiome is composed of tumor type-specific intracellular bacteria. *Science* **368**, 973-980 (2020).

30. G. D. Poore *et al.*, Microbiome analyses of blood and tissues suggest cancer diagnostic approach. *Nature* **579**, 567-574 (2020).

31. A. Fu *et al.*, Tumor-resident intracellular microbiota promotes metastatic colonization in breast cancer. *Cell* **185**, 1356-1372 e1326 (2022).

32. M. Meisel *et al.*, Microbial signals drive pre-leukaemic myeloproliferation in a Tet2-deficient host. *Nature* **557**, 580-584 (2018).

33. I. Campedelli *et al.*, Genus-Wide Assessment of Antibiotic Resistance in Lactobacillus spp. *Appl Environ Microbiol* **85**, (2019).

34. S. C. Choi *et al.*, Gut microbiota dysbiosis and altered tryptophan catabolism contribute to autoimmunity in lupus-susceptible mice. *Sci Transl Med* **12**, eaax2220 (2020).

35. I. Klare *et al.*, Antimicrobial susceptibilities of Lactobacillus, Pediococcus and Lactococcus human isolates and cultures intended for probiotic or nutritional use. *J Antimicrob Chemother* **59**, 900-912 (2007).

36. J. Wang *et al.*, UV-induced somatic mutations elicit a functional T cell response in the YUMMER1.7 mouse melanoma model. *Pigment Cell Melanoma Res* **30**, 428-435 (2017).

37. L. Cervantes-Barragan *et al.*, Lactobacillus reuteri induces gut intraepithelial CD4(+)CD8alphaalpha(+) T cells. *Science* **357**, 806-810 (2017).

38. T. Zelante *et al.*, Tryptophan catabolites from microbiota engage aryl hydrocarbon receptor and balance mucosal reactivity via interleukin-22. *Immunity* **39**, 372-385 (2013).

39. M. Veldhoen *et al.*, The aryl hydrocarbon receptor links TH17-cell-mediated autoimmunity to environmental toxins. *Nature* **453**, 106-109 (2008).

40. F. J. Quintana *et al.*, Control of T(reg) and T(H)17 cell differentiation by the aryl hydrocarbon receptor. *Nature* **453**, 65-71 (2008).

41. H. M. Roager, T. R. Licht, Microbial tryptophan catabolites in health and disease. *Nat Commun* **9**, 3294 (2018).

42. S. Spranger *et al.*, Mechanism of tumor rejection with doublets of CTLA-4, PD-1/PD-L1, or IDO blockade involves restored IL-2 production and proliferation of CD8(+) T cells directly within the tumor microenvironment. *J Immunother Cancer* **2**, 3 (2014).

43. Van den Eynde et al., Is There a Clinical Future for IDO1 Inhibitors After the Failure of Epacadostat in Melanoma? *Annual Review of Cancer Biology* **4**, 241-256 (2020).

44. K. Hezaveh *et al.*, Tryptophan-derived microbial metabolites activate the aryl hydrocarbon receptor in tumor-associated macrophages to suppress anti-tumor immunity. *Immunity* **55**, 324-340 e328 (2022).

45. G. Reuter, The Lactobacillus and Bifidobacterium microflora of the human intestine: composition and succession. *Curr Issues Intest Microbiol* **2**, 43-53 (2001).

Materials And Methods

Melanoma patient serum samples

Study design, baseline clinical and demographic characteristics, assessments and definition of endpoints of a cohort of advanced stage IV melanoma patients was recently described in (*1*). Briefly, clinical data and sera of advanced stage IV melanoma patients that either responded (referred to as responders (R)) = partial response or complete response, n = 19) or failed to respond (referred to as non-responders (NR) = stable disease or progressive disease, n = 23) to combinatorial IFNa and aPD1 were used in this study (ClinialTrials.gov identifier: NCT02112032; KEYNOTE-020). Collected serum samples at baseline in treatment naïve patients were used to analyze systemic I3A and kynurenine by mass spectroscopy. Approval to treat patients was obtained from the University of Pittsburgh's Hillman Cancer Center (HCC) Institutional Review Board (No. PRO14030075).

Animals

C57BL/6 mice were obtained from The Jackson Laboratory. *Ifng*$^{L-}$ *E8I Cre* mice were provided by Dr. Dario A. A. Vignali, University of Pittsburgh, and *Rag2*$^{-/-}$ mice were kindly provided by Dr. M. Shlomchik, University of Pittsburgh. *Ahr*^{fl} CD8 *Cre* mice were generated by crossing *Ahr*^{fl} (*Ahr*$^{tm3.1Bra}$/J, The Jackson Laboratory, 006203) mice with CD8a-*Cre* (C57BL/6-Tg(Cd8a-cre)1Itan/J, The Jackson Laboratory, 008766) mice. For all experiments, 6-10 week-old females or males were used; no notable sex-dependent differences were found for the reported experiments. Mice were housed at the University of Pittsburgh animal facilities under specific pathogen-free (SPF) conditions, where cages were changed on a weekly basis. Ventilated cages, bedding, food and water (non-acidified) were autoclaved before use, ambient temperature maintained at 23 °C, and 5% Clidox-S was used as a disinfectant. Experimental and breeding cages were randomly housed on two different racks in the vivarium, and all cages were kept on automatic

12-h light/dark cycles. Animal care and experimentation were conducted in accordance with NIH guidelines and approved by the Institutional Animal Care and Use Committee at the University of Pittsburgh.

Gnotobiotic animal husbandry

Food, bedding, and water (non-acidified) were autoclaved before transfer into the sterile isolators. Cages within isolators were changed weekly, and all the cages in the vivarium were kept on 12-h light/dark cycles. Microbiology testing of fecal (experimental mice) or of cecum samples (sentinel mice; aerobic and anaerobic culture, 16S qPCR) was performed every other week to confirm germ-free status.

Tumor models

On day zero mice were injected subcutaneously in the right hind flank with 10^6 B16-F0 (ATCC, CRL-6322), 10^6 YUMM1.7 (ATCC, CRL-3362), or 5 x 10^5 MC38 (Kerafast, ENH204-FP) tumor cells in 100 µL sterile PBS. Tumor volumes were calculated using the formula *tumor volume= length x width*^{2}*x 0.5*, where length represents the largest tumor diameter and width represents the diameter perpendicular to the length (*2*). For survival experiments mice were sacrificed when tumors reached a volume of ³ 6000 mm^3.

Administration of bacteria, I3A, KYN, and antibiotics

Lactobacillus reuteri DArAT lacking the gene coding for aromatic amino acid aminotransferase class I/II (*3*) was generously provided by Dr. L. Cervantes-Barragan, Emory University. *Lactobacillus reuteri* (ATCC, BAA-2837, isolated from human breast milk), *Lactobacillus johnsonii* (ATCC BAA-3147), *Bifidobacterium longum Reuter* (ATCC, BAA-999), and *Lactobacillus reuteri* DArAT were cultured anaerobically in MRS Broth (BD Difco, DF0881-17-5) at 37°C. *Escherichia coli* (ATCC, BAA-1429) was cultured aerobically in Tryptic Soy Broth (BD Bacto, DF0370-17-3) at 37°C. Briefly, for oral gavage experiments mice were gavaged daily with 10^9 colony forming units (CFU) bacteria in 200 µL PBS, or 20 mg/kg body weight (b.w.) or 40 mg/kg b.w Indole-3-Aldehyde (Sigma-Aldrich, 129445) in 200 µL corn oil, or vehicle control starting one day post tumor cell engraftment until endpoint analysis (EPA) unless noted otherwise. For heat-killed experiments, bacteria were incubated at 95 °C for 150 minutes (min) prior to gavage. For intratumoral injection experiments, mice were injected with 2x10^7 CFU viable or heat-killed *L. reuteri* or *E. coli* in 40 µL PTT, 10 µM, 1000 µM, or 200µg/mL I3A or L-kynurenine (Sigma-Aldrich, K8625) in 40 µL 10% Tween 20, 0.5 mg/mL ampicillin (Fisher BioReagents, BP1760-25) or vancomycin (Sigma-Aldrich, V2002) in 40 µL sterile water, or vehicle control starting when tumors reached an average volume of 300 mm^3 every three days until EPA unless indicated otherwise.

In vitro assessment of ampicillin and vancomycin effectiveness against *L. reuteri*

5 x 10^7 CFU *L. reuteri* were inoculated in MRS broth containing 0.5 mg/mL ampicillin or vancomycin or vehicle control (sterile water). Cultures were grown anaerobically at 37 °C for 24 hours (h). Cultures were

plated on MRS agar and incubated at 37 °C for 24 h under anaerobic conditions. CFU were then quantified.

CD8/CD4 T cell depletion and anti-PD-L1 mAb immunotherapy

For depletion of CD8/CD4 T Cells mice were injected intraperitoneally weekly with 250 µg *InVivoMAb* anti-mouse CD8a (BioXCell, BE0061), *InVivoMAb* anti-mouse CD4 (BioXcell, BE0003-1), or isotype control (BioXCell, BE0090) for a total of three times. For anti-PD-L1 mAb immunotherapy experiments, mice were injected intraperitoneally on day 5, 7, 9, and 12, with 100 µg *InVivoMAb* anti-mouse PD-L1 (BioXCell, BE0101) or *InVivoMAb* rat IgG2b isotype control (BioXCell, BE0090).

Tissue harvest and cell purification

Tumors and spleens were harvested with autoclaved tools under sterile conditions and weight was recorded. Spleens were mashed and underwent erythrocyte lysis using the Mouse Erythrocyte Lysing Kit (R&D Systems, WL2000) and remaining cells were used for flow cytometry analysis. Tumor-intrinsic lymphocytes were isolated via purification of mononuclear cells using 40% percoll centrifugation (Cytiva, 17089101), subsequent erythrocyte lysis, and an enrichment of $CD45^+$ cells as described: cells were incubated for 5 min on ice with rat serum and Fc block (BD Biosciences, 553142), followed by a 15 min incubation on ice with biotinylated anti-CD45 (Biolegend, 103104). Cells were washed, and incubated with streptavidin beads (BD Biosciences, 557812) for 20 min, followed by a 5 min incubation in an EasySep magnet (STEMCELL, 18000). Cells poured out from the magnet were discarded, and cells remaining were used for flow cytometry analysis.

Flow cytometry

Single-cell suspensions were prepared as described above and resuspended in FACS buffer (PBS, 2% FCS) for immunostaining and subsequent FACS analysis. Cell suspensions were incubated with Fc Block (BD Biosciences, 553142), followed with surface marker antibody (Ab) stain for 20 min at 4 °C. Abs were used as follows: anti-CD45 (BV480, BD Biosciences, 566095), anti-TCRb (Alexa Fluor® 700, BD Biosciences, 560705), anti-CD4 (BV650, BD Biosciences, 563232), anti-CD8 (BV570, BioLegend, 100740), anti- I-A/I-E (BUV496, BD Biosciences, 750281), anti-Ly-6G/Ly-6C (Alexa Fluor® 700, BioLegend, 108422), anti-CD11c (FITC, BioLegend, 117306), anti-CD11b (APC-eFluor 780, eBioscience, 47-0112-80), anti-F4/80 (PE-Cyanine5, eBioscience, 15-4801-80). For dead cell exclusion, cells were stained with Zombie NIR Fixable Viability dye (BioLegend, 423105) for 10 min at 4 °C and washed in FACS buffer. For intracellular cytokine and transcription factor staining, surface Ab-stained cells were first fixed and permeabilized using the FoxP3 Transcription Factor Staining Buffer kit (eBioscience, 00-5523-00) following manufacturer's instructions. Cells were further stained with Abs against intracellular proteins for 30 min at 4 °C. Abs were used as follows: anti-IFNg (BV605, BioLegend, 505839), anti-FoxP3 (FITC, eBioscience, 11-5773-82), anti-Granzyme B (PE, eBioscience, 12-8898-80), anti-Ki67 (PE-eFluor 610, eBioscience, 61-5698-82). Samples were FSC-A/SSC-A gated to exclude debris and gated to exclude dead cells. Samples were run on an Aurora (Cytek) flow cytometer and analyzed with FlowJo 10 (Tree Star).

Single-cell RNA sequencing sample preparation

Single-cell suspensions from tumors (n = 4 per condition) were prepared as described above except as follows. Cells were purified via an enrichment for CD90.2$^+$ cells using EasySep™ Mouse CD90.2 Positive Selection Kit II (STEMCELL, 18951). Samples were stained using anti-TCRβ (Alexa Fluor® 700, BD Biosciences, 560705), anti-CD4 (BUV395, BD Biosciences, 563790), anti-CD8a (BUV737, BD Biosciences, 612759), and each sample was stained with TotalSeq™-C03NN anti-mouse Hashtag 1 Antibodies with unique hashtag oligonucleotides (HTOs) in staining buffer for 30 min on ice (Biolegend Cat # 155861, 155863, 155865, 155867, 155871, 155873, 155875, 155877). For dead cell exclusion, cells were stained with LIVE/DEAD™ Fixable Aqua Dead Cell Stain Kit (Invitrogen, L34957) for 10 min on ice. Doublets and dead cells were excluded. From each animal, 8,000 CD8$^+$ live cells were sorted using a 5-laser Aria-10 cytometer, and samples from the same condition were pooled in PBS + 0.04% BSA. GEM formation and library preparation was performed using Chromium Next GEM Single Cell 5' v2 workflow from 10x Genomics (Chromium Next GEM Single Cell 5' Kit v2, 16 rxns PN-1000263, Library Construction Kit, 16 rxns PN-1000190, 5' Feature Barcode Kit, 16 rxns PN-1000256, Chromium Next GEM Chip K Single Cell Kit, 48 rxns PN-1000286, Dual Index Kit TT Set A, 96 rxns PN-1000215, Dual Index Kit TN Set A, 96 rxns PN-1000250). Hashtagged cells from 8 mice (4 PBS treated and 4 *L. reuteri* treated) were pooled onto a single lane of the 10x chip to allow sample multiplexing. Prepared libraries were quality-checked on Agilent TapeStation and sequenced on HiSeq4000 (Novogene Inc).

Single-cell RNA sequencing analysis

Sequencing data were downloaded from Novogene onto the Joglekar laboratory server. Reads were aligned with CellRanger-4.0.0 to the *Mus musculus* reference genome (mm10-2020-A). Hashtag oligonucleotide sequences were added in the feature reference file included in the *cellranger count* step. Following alignment and generation of gene expression matrix, samples were processed in Seurat v4.0.1 (*4*). We used Seurat's hashtag demultiplexing workflow to read hashtag oligos (*HTODemux*). Data from the resultant HTOs were re-processed and re-demultiplexed for further analysis. First, data were normalized, and integration anchors were identified. Integrated data were scaled and used for downstream Principle Component Analysis and visualization using Uniform Manifold Approximation Embedding (UMAP). First 20 principle components were used to derive Seurat clusters. Differential gene expression analysis was performed using the *FindMarkers* function in Seurat using *negbinom* testing. Trajectory analyses were performed using Monocle 3 (*5, 6*). Visualization and all statistical testing was performed in *RStudio* running on R version 4.0.3.

In vivo intestinal permeability measurement

To determine intestinal epithelial barrier permeability in mice, FITC-labelled dextran method was used as previously described (*7*). In brief, mice were withheld from food and water for 4 hours upon which they were gavaged with 60mg/100g body weight Fluorescein isothiocyanate (FITC)–dextran (MW 4,000, Sigma-Aldrich, 46944). After 3 h blood was collected by cheek bleeding, spun at 10,000 rpm for 10 min at

4 C, and 50 µL plasma was added to a 96-well flat bottom plate (Corning, 07-200-656) in duplicate. Analysis of FITC–dextran concentration was performed with a fluorescence spectrophotometer setup (SpectraMax® i3x using SoftMax Pro 3.0.7 Software) under the following settings: read type endpoint at excitation wavelength 485 and emission wavelength 520 (bandwidth 15), flashes per well 6, read height 4 mm. FITC-dextran concentration was determined in samples from a standard curve generated by serial dilution of FITC-dextran.

RNA processing and RT-PCR

A piece of the jejunum and colon (~5 mm) was incubated in RNAlater™ (Qiagen) at 4 °C for 48 h and stored at -80 °C until further analysis. For RNA extraction a Tissue-Tearor Homogenizer (Biospec) was used. RNA was extracted using the RNeasy Mini Kit (Qiagen). cDNA synthesis was performed using iScript™ cDNA Synthesis Kit (Bio-Rad) according to manufacturer's instructions. Expression analysis was performed in duplicate via real-time PCR on a BioRad CFX384 Touch™ Real-Time PCR Detection System using iTaq™ Universal SYBR (Bio-Rad). Expression levels were quantified and normalized to *Gapdh* expression.

AhR agonist containing supernatant

Similar to previously described (*3*), to generate AhR agonist containing supernatants, *L. reuteri* WT or *L. reuteri* DArAT were grown in MRS broth overnight, harvested by centrifugation, washed with PBS, and 10^{10} CFU were inoculated into sterile 10 mL of peptone-tryptone water (10 g/L peptone and 10 g/L tryptone, 5 g/L NaCl) supplemented with 0.6 mM L-tryptophan. After a 14 h incubation at 37 °C under anaerobic conditions, bacteria were centrifuged (5000 x *g*, 10 min), supernatant collected and filter sterilized (0.2 mm pore diameter cellulose acetate filter (VWR)) and stored at -80 °C until further use. For *in vitro* experiments, supernatants were added to cells at a final concentration of 10% vol/vol in culture media (*3*).

In vitro naïve CD8 T cell stimulation

Naïve CD8 T cells were purified with EasySep™ Mouse Naïve CD8 T Cell Isolation Kit (STEMCELL, 19858). 5 x 10^5 naïve CD8 T cells were stimulated with plate coated anti-CD3 (BD Biosciences, 553057) and soluble anti-CD28 (BD Biosciences, 553294) (each 1 µg/mL) in the presence of 10% *L. reuteri* WT- or 10% *L. reuteri* DArAT-supernatant. Amount of produced IFNg in the supernatant after 72 h was assessed by ELISA.

Enzyme-linked immunosorbent assay (ELISA) to measure IFNg

In vitro T cell supernatants were used to measure IFNg according to manufacturer's instructions. Briefly, ELISA plates were coated overnight at 4 °C with 0.5 µg/ml IFNg (BD Pharmingen, 551309). Plates were washed once (0.05% Tween 20 in PBS) and blocked for 1 h with blocking buffer (5% FBS in PBS). Standards and samples were incubated overnight at 4 °C. Plates were washed and incubated with biotin-

conjugated IFNg detection AB (0.5 µg/ml, BD Pharmingen, 554410) for 1 h at room temperature (RT). Plates were then washed and incubated with Horseradish Peroxidase-conjugated streptavidin (Jackson ImmunoResearch, 016-030-084) for 10 min followed by washing and development with TMB substrate (Pierce, 34021). Reactions were stopped by the addition of 2N H_2SO_4, and absorbance was measured at 450 nm on a SpectraMax i3 plate reader (Molecular Devices). IFNg concentration in supernatants was determined from a standard curve generated by serial dilution of IFNg.

AhR activity assay

Luciferase-expressing HT29-Lucia™ AhR reporter cells under the control of *Cyp1a1* gene promoter (referred to as "AhR reporter cells") were purchased from InvivoGen (ht2l-ahr). Cells were cultured in DMEM (Gibco) supplemented with 10% FBS, 1 x Penicillin-Streptomycin-Glutamine (Gibco), 100 µg/mL Normocin (InvivoGen), and 100 µg/mL selective antibiotic Zeocin (InvivoGen). Briefly, 20 µL of sample was incubated with approximately 50,000 AhR reporter cells for 24 h. Following incubation, 20 µL of supernatant was transferred into a 96-Well Clear Bottom Black Microplate (Corning) and 50 µL QUANTI-Luc™ (InvivoGen) was added. Samples were immediately read for luminescence via a SpectraMax® i3x using SoftMax Pro 3.0.7 Software under the following settings: read type endpoint at all wavelengths, integration time 100 ms, read height 2 mm.

AhR activity measurement in tumor homogenate

Pieces of tumor (~ 200 mg) were removed and mashed through 100 µm cell strainers in sterile PBS, followed by centrifugation at 1800 rpm for 5 min to pellet cells. Supernatant was collected and measured for AhR activity using AhR reporter cells.

Bacterial cultures from tumors

Tumors were aseptically removed, weighed, and homogenized via mashing through a 100 µm cell strainer in 2 mL sterile water containing 0.05% NP-40 (Sigma). Bacterial expansion was performed under anaerobic conditions at 37 °C as follows. After a 1 h incubation, 10 mL MRS or Tryptic Soy broth was added to each sample followed by an additional 12 h incubation, after which the expansion and subsequent serial dilutions were plated on MRS or Tryptic Soy agar. Plates were incubated anaerobically for 24 h. Similar as previously described (*7*), CFUs were then quantified and single colonies were picked for 16S rRNA amplicon sequencing. In Fig. 3D where mice were treated with *L. reuteri* WT or *L. reuteri* DArAT additional single colonies were picked for strain specific PCR, where deletion, or lack of deletion, of Lreu23DRAFT_RS05825 was verified using primers 5'-CGACTTGGTGGTCAAAGCGG-3' and 5'-CATTGCTACCCACTTCCTTTACG-3' (*3*).

AhR activity measurement in translocated bacteria in the tumor

For assessments of AhR activity, MRS-broth-expanded cultures described above were pelleted at 5000 x *g* for 10 min, resuspended in peptone-tryptone-tryptophan (PTT) media, and cultured anaerobically at 37 °C,

shaking at 250 rpm, for 14 h. Bacteria were again pelleted and supernatant was collected and measured for AhR activity.

Bacterial colony identification

Bacterial colonies were identified as described in (*7*). In brief, grown colonies were picked with sterile pipette tips and stored at -80 °C until analysis. At day of analysis, picked bacterial colonies were thawed at RT, resuspended with 20 µL of sterile water and lysed at 95 °C for 10 min. Samples were subsequently cooled down to 4 °C and then the DNA (2 µl) was used as template DNA in PCR reactions amplifying the 16S rRNA gene using universal bacterial 16S rRNA primers (27F, 5'-AGAGTTTGATCMTGGCTCAG-3' and 1525R, 5'-AAGGAGGTGATCCAGCC-3') with reaction conditions: 95 °C for 5 min followed by 35 cycles of 95 °C for 30 sec, 55 °C for 30 sec, 72 °C for 2 min and then 72 °C for 20 min. The amplification product (8 µl) was incubated with 2 µl ExoSAP-IT™ (ThermoFisher) for 37 °C for 15 min, followed by 80 °C for 15 min. As recently described (*7*), amplicons were sequenced by capillary sequencing, and the resulting sequences were analyzed using BLASTN and the 16S ribosomal RNA sequences NCBI database for species identification.

DNA extraction from intestinal contents and feces

The Fast DNA Stool Mini Kit (Qiagen) was used to extract total DNA from intestinal contents and feces. Quantitative PCR (qPCR) was performed as recently described (*8*). Briefly, qPCR was performed on a Bio-Rad CFX384 Touch™ Real-Time PCR Detection System using iTaq™ Universal SYBR (Bio-Rad, 1725125) using primers as follows: 16S rRNA-encoding gene (340F, 5’-ACTCCTACGGGAGGCAGCAGT-3’ and 514R, 5’-ATTACCGCGGCTGCTGGC-3’), *Lactobacillus reuteri* (F, 5’-TTGGAAATGTTCCACAAGAC-3’ and R, 5’-TTGTGAGTTTGGATTGAACC-3), mouse *Ifnb1* (F, 5’- CCATCCAAGAGATGCTCCAG-3’ and R, 5’-GTGGAGAGCAGTTGAGGACA-3’). Reactions were run at 95 °C for 3 min, followed by 40 cycles of 95 °C for 15 min and 63 °C for 60 seconds. Expression levels of *16S rRNA*-encoding gene and *Lactobacillus reuteri* were quantified and normalized to *Ifnb1* expression.

Dietary experiments

For non-dietary experiments, mice were fed with irradiated standard chow (Prolab, RMH 3000) *ad libitum* that contains approximately 0.28% tryptophan. For dietary experiments, tryptophan-modified synthetic chows that differ only by their tryptophan content (0.19% or 1.19%; A11022501-02, Research Diets) were fed to mice for the indicated periods of time (*ad libitum*). Overall food consumption was similar across chows.

Sample preparation of untargeted high-resolution LC-HRMS

Metabolic quenching and polar metabolite pool extraction was performed by adding 360 µL ice cold methanol containing 10 µM $^{13}C_1$-creatine (Sigma-Aldrich, Boston MA) to 90 µL sample. After 3 min of vortexing, the supernatant was cleared of protein by centrifugation at 16,000 x g. 450 µL cleared

supernatant was dried to completion under nitrogen gas and resuspended in 90 µL water. 2 µL of resuspended sample was subjected to online LC-MS analysis. Molar quantities were calculated using a calibration curve using purified kynurenine (Kyn) and indole-3-carboxaldehyde (I3A, Sigma-Aldrich) in a 1:3 series dilution from 25 µM to 11 nM.

Untargeted high-resolution LC-HRMS

Analyses were performed by untargeted LC-HRMS. Briefly, samples were injected via a Thermo Vanquish UHPLC and separated over a reversed phase Phenomenex Kinetix C18 column (2.1 × 150mm, 1.7 µm particle size) maintained at 55 °C. For the 10 min LC gradient, the mobile phase consisted of the following: solvent A (water / 5 mM ammonium formate / 0.1% formic acid) and solvent B (methanol / 0.1% formic acid). The gradient was the following: 0 - 0.3 min 3% B, increase to 30 % B over 0.5 min, continue increasing to 60% B over 1 min, hold at 60 % B for 1.3 min, increase to 95% B over 0.5 min, hold at 95% B for 1.4 min, equilibrate at 3% B for 4.5 min. The Thermo IDX tribrid mass spectrometer was operated in positive ion mode, scanning in ddMS2 mode (2 µscans) from 70 to 800 m/z at 120,000 resolution with an AGC target of 2e5 for full scan, 2e4 for ms2 scans using HCD fragmentation at stepped 15,35,50 collision energies. Source ionization setting was 3.0 kV spray voltage for positive mode. Source gas parameters were 35 sheath gas, 12 auxiliary gas at 320 °C, and 8 sweep gas. Calibration was performed prior to analysis using the PierceTM FlexMix Ion Calibration Solutions (Thermo Fisher Scientific). Integrated peak areas were then extracted manually using Quan Browser (Thermo Fisher Xcalibur ver. 2.7). Purified standards were then purchased and compared in retention time, m/z, along with ms2 fragmentation patterns to validate the identity of peaks.

Statistical analysis

The majority of experiments were repeated at least two times to obtain data for indicated statistical analyses. Mice were allocated to experimental groups on the basis of their genotype and randomized within the given sex- and age-matched group. Given that our mice were inbred and matched for age and sex, we assumed similar variance between the different experimental groups. Statistically significant outliers were excluded from analysis. We did not perform a priori sample size estimation but always used as many mice per group as possible in an attempt to minimize type I and type II errors. Except mass spectroscopical (LC-HRMS) analysis, investigators were not blinded during experiments and outcome assessment. All experimental and control animals were littermates and none were excluded from the analysis at the time of harvest. All quantitative data are presented as mean ± standard error of the mean (SEM), unless otherwise indicated. Data was analyzed using an unpaired two-tailed Student's *t*-test for single comparisons, and one-way or 2-way ANOVA for multiple comparisons. ANOVA analysis was followed by a Sidak's post-hoc test. Correlations were calculated using the Spearman correlation. Figures and statistical analysis were generated using GraphPad Prism 9 (GraphPad Software). The statistical test used, and P values are indicated in each figure legend. P values of < 0.05 were considered statistically significant. $^{*}P < 0.05$, $^{**}P < 0.01$, $^{***}P < 0.001$ and $^{****}P < 0.0001$.

Data and materials availability: All data are available in the main text or the supplementary materials, except raw CD8 T cell single-cell data, which is available upon request.

Materials and Methods References:

1. D. Davar *et al.*, Phase Ib/II Study of Pembrolizumab and Pegylated-Interferon Alfa-2b in Advanced Melanoma. *J Clin Oncol*, JCO1800632 (2018).

2. A. Sivan *et al.*, Commensal Bifidobacterium promotes antitumor immunity and facilitates anti-PD-L1 efficacy. *Science* **350**, 1084-1089 (2015).

3. L. Cervantes-Barragan *et al.*, Lactobacillus reuteri induces gut intraepithelial CD4(+)CD8alphaalpha(+) T cells. *Science* **357**, 806-810 (2017).

4. Y. Hao *et al.*, Integrated analysis of multimodal single-cell data. *Cell* **184**, 3573-3587 e3529 (2021).

5. C. Trapnell *et al.*, The dynamics and regulators of cell fate decisions are revealed by pseudotemporal ordering of single cells. *Nat Biotechnol* **32**, 381-386 (2014).

6. J. Cao *et al.*, The single-cell transcriptional landscape of mammalian organogenesis. *Nature* **566**, 496-502 (2019).

7. M. Meisel *et al.*, Microbial signals drive pre-leukaemic myeloproliferation in a Tet2-deficient host. *Nature* **557**, 580-584 (2018).

8. M. Meisel *et al.*, Interleukin-15 promotes intestinal dysbiosis with butyrate deficiency associated with increased susceptibility to colitis. *ISME J* **11**, 15-30 (2017).

Declarations

Acknowledgments: We thank the *Unified Flow Core* at the Department of Immunology, University of Pittsburgh for flow cytometry sorting and resources. We thank the *Single Cell Core* at the University of Pittsburgh for performing 10x genomic workflow and library generation. We thank the *Gnotobiotic Core Facility* at the University of Pittsburgh for their service. We thank the *Metabolomics and Lipidomics Core* at the University of Pittsburgh for their service. **Funding:** This work was supported by an Investigator Start-up Fund, Department of Immunology, University of Pittsburgh School of Medicine to M.M and R.H; a Hillman Developmental Pilot Award (NIH/NCI P30 CA047904) to M.M. and A.V.J; a NIH/NIDDK R01 DK130897, a NIH/NCI R21 CA259636, and a Melanoma Research Alliance award https://doi.org/10.48050/pc.gr.143738 (820677) to M.M.; T32 CA082084 to A.C.M; F32 CA247004-01, T32 CA082084 to A.M.G.D; P01 AI108545 and R01 CA203689 to D.A.A.V; a NIH R21AI163721 grant and a Hillman Developmental Pilot Award (NIH/NCI P30 CA047904) to R.H.; a NIHS10OD023402 grant to S.G.W.

Author contributions: M.J.B. performed majority of experiments and data analyses and wrote draft of the manuscript. A.C.M. performed majority of experiments and data analyses and helped review and edit the manuscript. C.M.P. and S.P.P. performed experiments and data analyses. J.S and M.R. helped with various experiments. S.J. M. and S. G. W. performed mass spectroscopy and data analyses. A.M.G.D. and D.A.A.V. provided *Ifng*$^{fl/fl}$ *E8I* Cre mice and provided feedback on manuscript. R.H. helped write the manuscript and provided feedback and advice on manuscript. A.V.J. provided advice on scRNA seq analysis experiment, performed computational scRNA seq analysis, and provided feedback and advice on manuscript. D.D. and H.M.Z. provided human serum samples. M.M. conceived and designed the research, guided the interpretation of the results, and wrote the manuscript.

Competing interests: DAAV: cofounder and stock holder – Novasenta and Tizona; stock holder - Oncorus and Werewolf; patents licensed and royalties - Astellas, BMS; scientific advisory board member - Tizona, Werewolf and F-Star; consultant - Astellas, BMS, Almirall, Incyte, Bicara; research funding - BMS, Astellas and Novasenta. A.V.J: Research funding – Mitsubishi Tanabe Pharma.

Additional Information: Supplementary Information is available for this paper.

Correspondence and requests for materials should be addressed to Marlies Meisel, Email: marlies@pitt.edu.

Figures

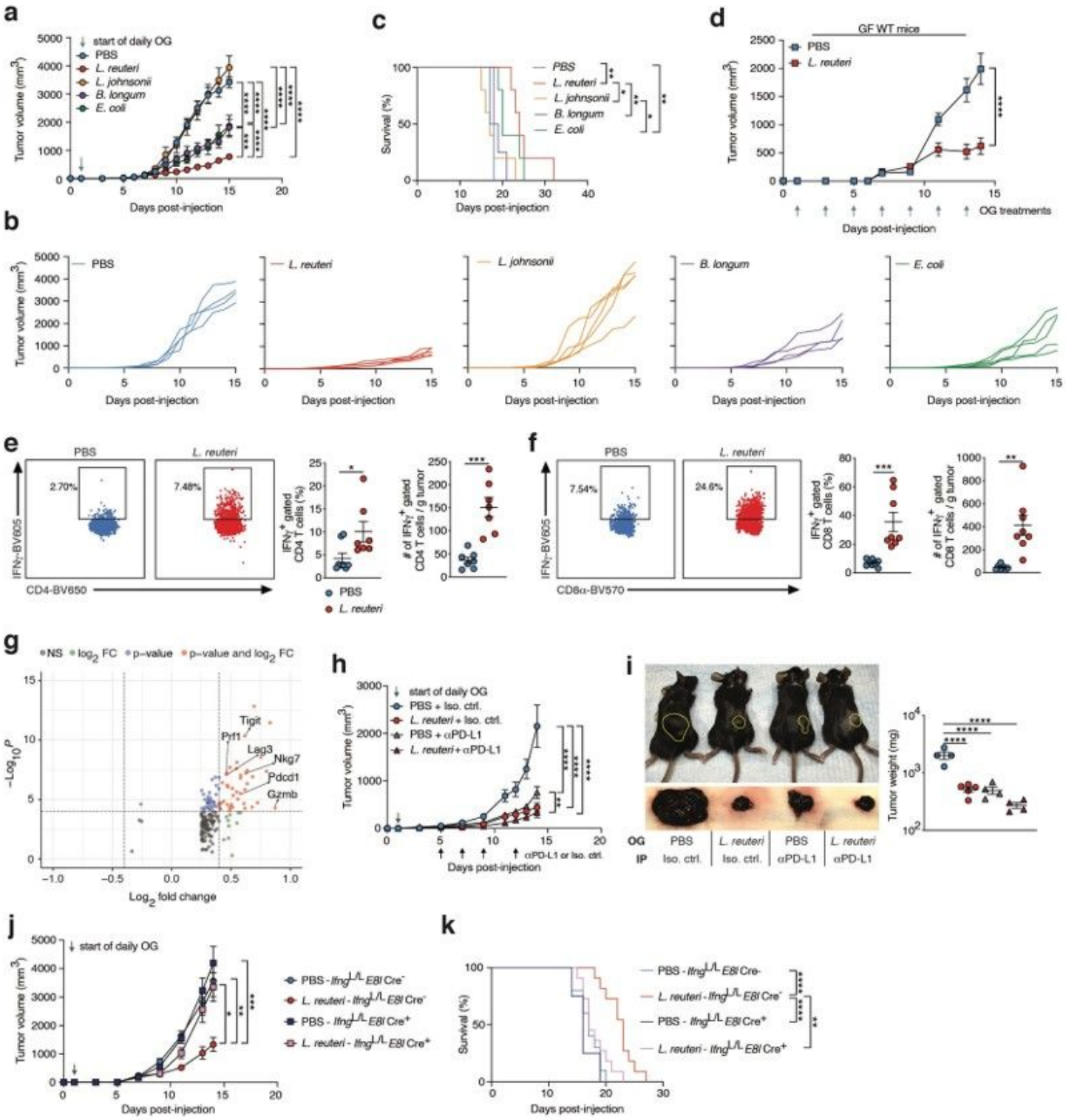

Figure 1

Orally administered *L. reuteri* potentiates ICI therapy efficacy in melanoma via an induction of interferon-g (IFNg)-producing CD8 T cells. (**a**) B16-F0 tumor growth of C57BL/6 WT mice orally administered *L. reuteri*, *L. johnsonii*, *B. longum, E. coli*, or vehicle control (PBS) daily starting one day post tumor cell engraftment (n = 4 (PBS), n = 5 (*L. reuteri*), n = 5 (*L. johnsonii*), n = 4 (*B. longum*), n = 5 (*E. coli*)). OG, oral gavage. (**b**) Individual tumor growth of mice from (a) by treatment group. (**c**) Survival analysis of mice

from (a). (**d**) B16-F0 tumor growth of germ-free (GF) mice orally administered *L. reuteri* or PBS every other day starting one day post tumor engraftment (n = 4 per group). (**e**-**f**) From left to right: representative plots, percentage, and total cells normalized to g tumor tissue of IFNg^{+} CD4 T cells (e) and IFNg^{+} CD8 T cells (f) within the tumor microenvironment (TME) of mice orally administered *L. reuteri* or PBS daily starting one day post tumor engraftment, assessed by flow cytometry on day 17 (D17) (n = 8 per group). (**g**) Differential gene expression analysis by negbinom testing of single-cell RNA-sequencing analysis of CD8 T cells isolated from the TME on D15 of mice orally administered *L. reuteri* or PBS daily starting one day post tumor cell engraftment. Selected genes representing effector (*Prf1*, *Nkg7*, and *GzmB*) and exhaustion (*Lag3*, *Tigit*, *Pdcd1*) markers are indicated in graph. FC, fold change (n = 4 per group). (**h**) B16-F0 tumor growth of mice orally administered *L. reuteri* or PBS daily starting one day post tumor cell engraftment and treated with intraperitoneal injections (IP) of aPD-L1 or isotype control (Iso. ctrl.) on D5, 7, 9 and 12 (n = 4 (PBS and Iso. ctrl.), n = 5 (*L. reuteri* and Iso. ctrl.), n = 4 (PBS and aPD-L1), n = 5 (*L. reuteri* and aPD-L1)). (**i**) (Left) representative images of tumor-bearing mice (top) and their respective tumors (bottom) and (right) tumor weights of mice from (h) on D14. Yellow circles outline tumor surface area. (**j**) B16-F0 tumor growth of *Ifng*$^{L/L}$ *E8I*-Cre^{+} and *Ifng*$^{L/L}$ *E8I* -Cre^{-} mice orally administered *L. reuteri* or PBS daily starting one day post tumor cell engraftment (n = 8 (*Ifng*$^{L/L}$ *E8I*-Cre^{+} PBS), n = 11 (*Ifng*$^{L/L}$ *E8I*-Cre^{+} *L. reuteri*), n = 10 (*Ifng*$^{L/L}$ *E8I*-Cre^{-} PBS), n = 11 (*Ifng*$^{L/L}$ *E8I*-Cre^{-} *L. reuteri*)). (**k**) Survival analysis of mice from (j). Data for (a), (d), (h), and (j) represent mean ± SEM analyzed by two-way analysis of variance (ANOVA) with Sidak's correction for multiple comparisons. Data for (c) and (k) represent comparison of survival curves analyzed by log-rank test. Data for (e) and (f) represent individual mice analyzed by unpaired *t* test. Mean ± SEM is shown. Data for (i) represents individual mice analyzed by one-way ANOVA with Sidak's correction for multiple comparisons. Mean ± SEM is shown. **P < 0.05, **P < 0.01, ***P < 0.001, ****P < 0.0001*.

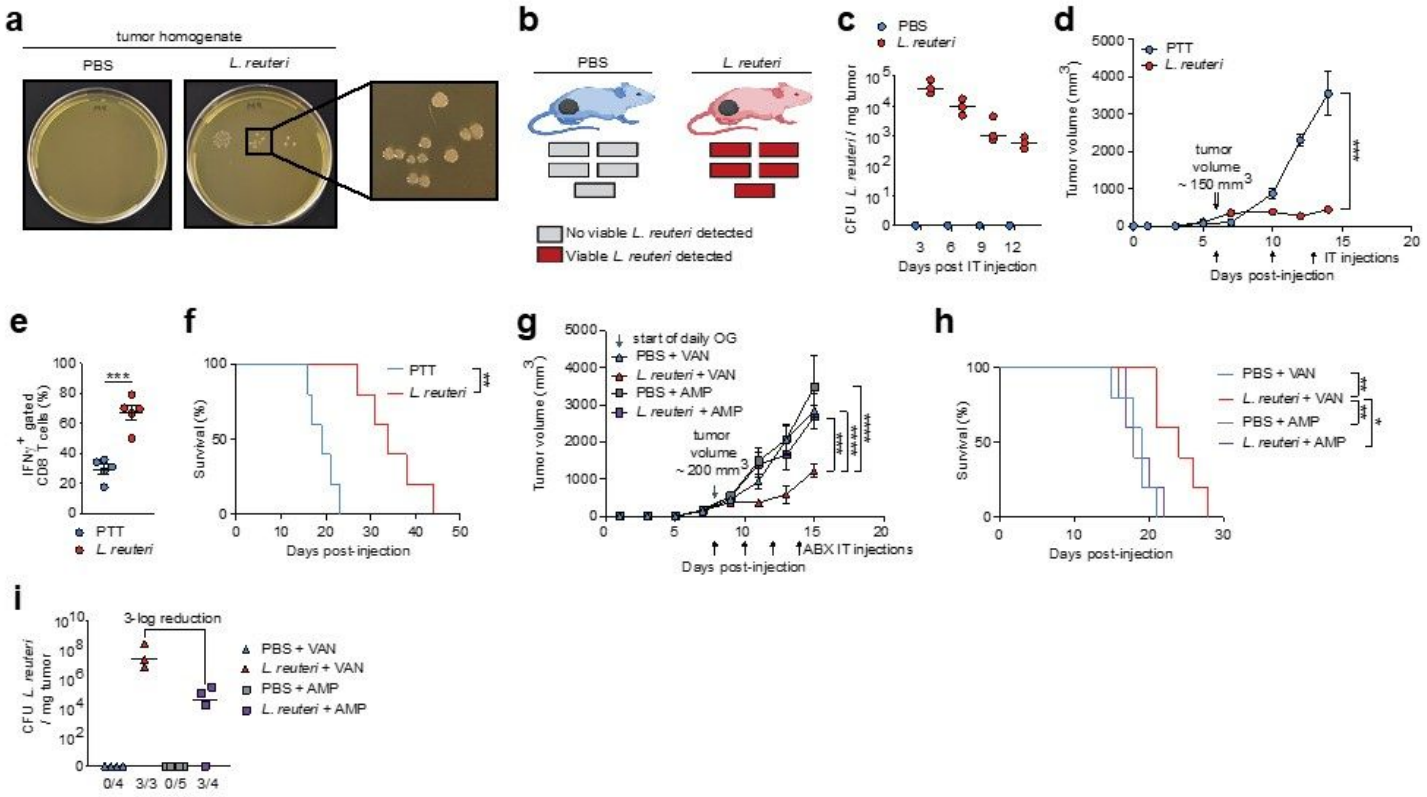

Figure 2

Intratumoral *L. reuteri* is necessary and sufficient to promote antitumor immunity in melanoma. (**a**-**b**) WT mice were orally administered *L. reuteri* or PBS for four consecutive days starting on D8 post B16-F0 tumor cell engraftment. Tumors were aseptically harvested for culture on D15 (n = 5 per group). Representative images of tumor homogenate cultures on MRS agar (a). Detection or failure to detect viable *L. reuteri* within the tumors of mice confirmed by 16S amplicon sequencing of individual colonies (b) (see also Extended Data Fig. 5a-b). (**c**) CFU quantification of *L. reuteri* per milligram tumor from mice intratumorally (IT) injected with *L. reuteri* or vehicle control (PBS) when tumors reached approximately 200 mm^3 and sacrificed at indicated time points following IT injection (n = 1 (PBS) per time point, n = 3 (*L. reuteri*) per time point). Median is shown. (**d**) B16-F0 tumor growth of mice IT injected with *L. reuteri* or peptone-tryptone-tryptophan media (PTT) on D6, 10, and 13 (n = 5 per group). (**e**) Percentage of $IFNg^+$ CD8 T cells within the TME of mice from (d) assessed by flow cytometry on D14. (**f**) Survival analysis of B16-F0 tumor-bearing mice IT injected with *L. reuteri* or PTT every 3 days starting when tumors reached approximately 350 mm^3 (D10) (n = 5 per group). (**g**) B16-F0 tumor growth of mice orally administered *L. reuteri* or PBS daily and IT injected with ampicillin (AMP) or vancomycin (VAN) every other day starting on D8 post tumor cell engraftment (n = 5 per group). ABX, antibiotics. (**h**) Survival analysis of mice from (g). (**i**) Quantification of CFU of *L. reuteri* per milligram tumor of mice from (g). *L. reuteri* presence was confirmed by 16S amplicon sequencing of individual colonies. Median is shown. (d) and (g) represent mean ± SEM analyzed by two-way ANOVA with Sidak's correction for multiple comparisons. Data for (e) represents individual mice analyzed by unpaired *t* test. Mean ± SEM is shown. Data for (f) and (h)

represent comparison of survival curves analyzed by log-rank test. **P < 0.05, **P < 0.01, ***P < 0.001, ****P < 0.0001.*

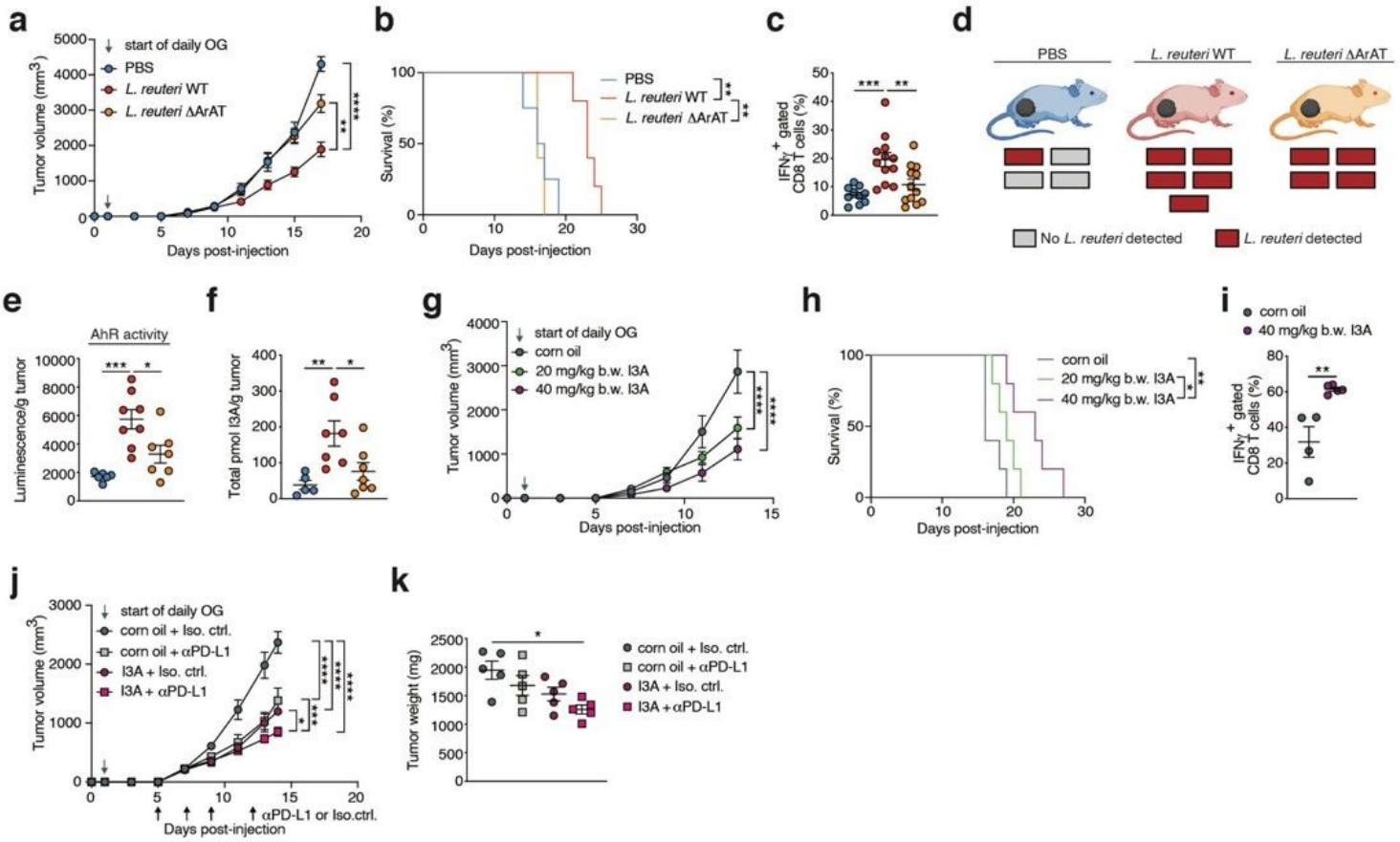

Figure 3

Production of AhR agonist indole-3-aldehyde by *L. reuteri* is required and sufficient to induce Tc1 cell effector function and restrain tumor outgrowth. (**a**) B16-F0 tumor growth of mice orally administered *L. reuteri* WT, *L. reuteri* DArAT, or PBS daily starting one day post tumor cell engraftment (n = 11 (PBS), n = 12 (*L. reuteri* WT), n = 12 (*L. reuteri* DArAT)). (**b**) Survival analysis of mice treated as in (a) (n = 5 per group). (**c**) Percentage of IFNg$^+$ CD8 T cells within the TME of mice from (a) assessed by flow cytometry on D17 post tumor cell engraftment. (**d**) Detection or failure to detect viable *L. reuteri* within the tumors of mice from (a). (**e**) AhR activity measured as luminescence normalized to g tumor derived from luciferase-expressing AhR reporter cells stimulated with tumor homogenate from mice treated as in (a) (n = 6 (PBS), n = 8 (*L. reuteri* WT), n = 7 (*L. reuteri* DArAT)). (**f**) Quantification of I3A pmol/g tumor of mice from (a) assessed by mass spectrometry. (**g**) B16-F0 tumor growth of mice orally administered I3A (20 mg/kg body weight (b.w.) or 40 mg/kg b.w.) or vehicle control (corn oil) daily starting one day post tumor cell engraftment (n = 5 per group). (**h**) Survival analysis of mice from (g). (**i**) Percentage of IFNg$^+$ CD8 T cells within the TME of mice orally administered 40 mg/kg b.w. I3A or corn oil for four consecutive days once tumors reached approximately 300mm^3 (D9), assessed by flow cytometry on D13 (n = 4 (corn oil) n = 5 (I3A)). (**j**) B16-F0 tumor growth of mice orally administered I3A (40 mg/kg b.w.) or corn oil daily starting

one day post tumor cell engraftment and treated IP with aPD-L1 or Iso. ctrl. on D5, 7, 9 and 12 (n = 5 per group). (**k**) Tumor weights of mice from (j) on D14. Data for (a), (g), and (j) represent mean ± SEM analyzed by two-way ANOVA with Sidak's correction for multiple comparisons. Data for (b) and (h) represent comparison of survival curves analyzed by log-rank test. Data for (c), (e), (f), and (k) represent individual mice analyzed by one-way ANOVA with Sidak's correction for multiple comparisons. Mean ± SEM is shown. Data for (i) represents individual mice analyzed by unpaired *t* test. Mean ± SEM is shown. **P < 0.05, **P < 0.01, ***P < 0.001, ****P < 0.0001.*

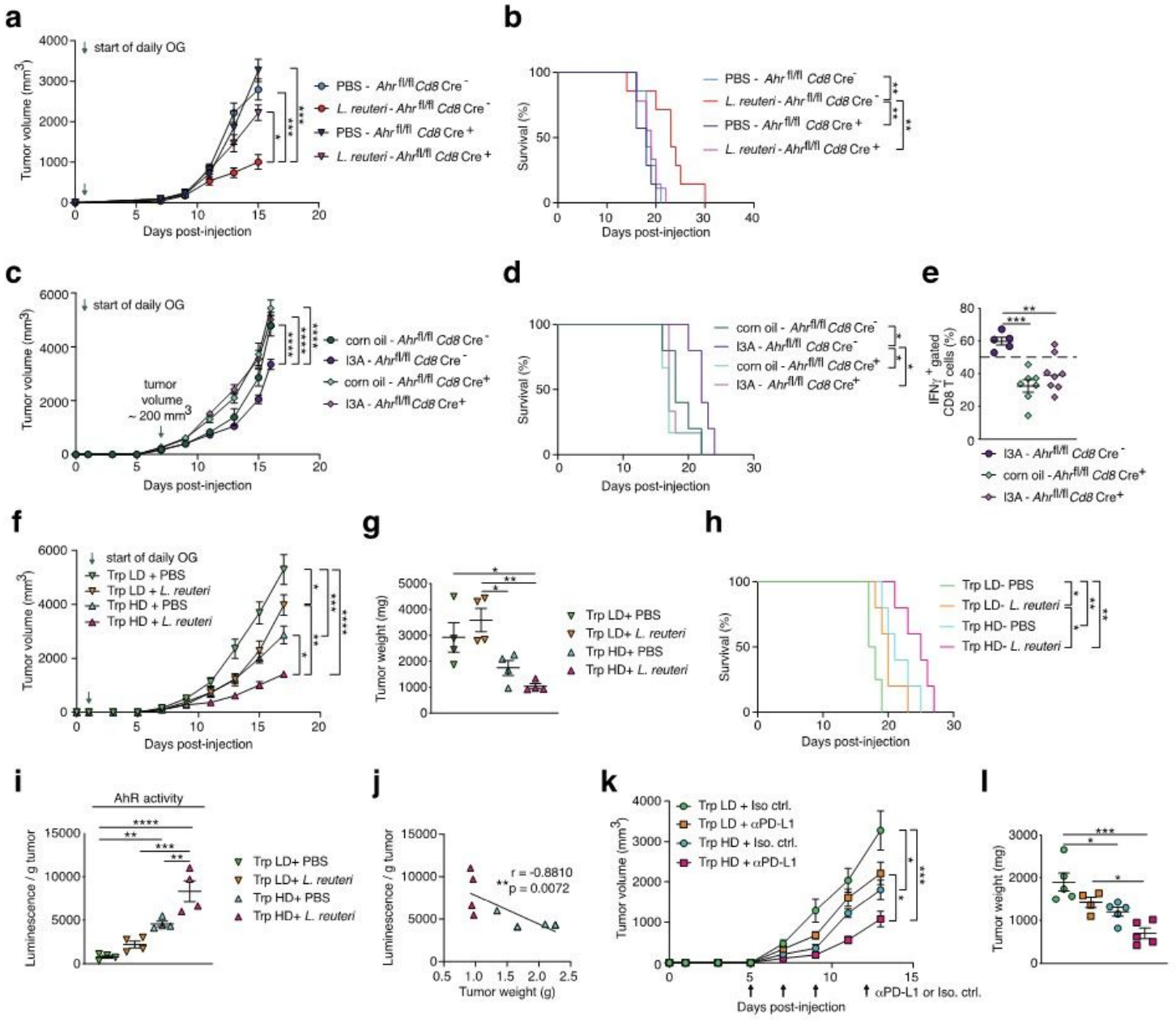

Figure 4

AhR expression in CD8 T cells is required for I3A-induced antitumor Tc1 cell effector function and a tryptophan-enriched diet is sufficient to facilitate ICI therapy. (**a**) B16-F0 tumor growth of *Ahr*$^{fl/fl}$ *Cd8*-Cre^{+} and *Ahr*$^{fl/fl}$ *Cd8*-Cre^{-} mice orally administered *L. reuteri* or PBS daily starting one day post tumor cell

engraftment (n = 7 (*Ahr*$^{fl/fl}$ *Cd8*-Cre^{+} PBS), n = 9 (*Ahr*$^{fl/fl}$ *Cd8*-Cre^{+} *L. reuteri*), n = 7 (*Ahr*$^{fl/fl}$ *Cd8*-Cre^{-} PBS), n = 6 (*Ahr*$^{fl/fl}$ *Cd8*-Cre^{-} *L. reuteri*)). (**b**) Survival analysis of mice from (a). (**c**) B16-F0 tumor growth of *Ahr*$^{fl/fl}$ *Cd8*-Cre^{+} and *Ahr*$^{fl/fl}$ *Cd8*-Cre^{-} mice orally administered I3A (40 mg/kg b.w.) or vehicle control (corn oil) daily starting once tumors reached approximately 200mm^{3} (D7) (n = 5 (*Ahr*$^{fl/fl}$ *Cd8*-Cre^{-} corn oil), n = 5 (*Ahr*$^{fl/fl}$ *Cd8*-Cre^{-} I3A), n = 6 (*Ahr*$^{fl/fl}$ *Cd8*-Cre^{+} corn oil), n = 7 (*Ahr*$^{fl/fl}$ *Cd8*-Cre^{+} I3A)). (**d**) Survival analysis of mice from (c). (**e**) Percentage of IFNg^{+} CD8 T cells within the TME of *Ahr*$^{fl/fl}$ *Cd8*-Cre^{+} and *Ahr*$^{fl/fl}$ *Cd8*-Cre^{-} mice orally administered 40 mg/kg b.w. I3A or corn oil for four consecutive days once tumors reached approximately 300mm^{3} (D8) and assessed by flow cytometry 24 hours post final treatment (D12). The dotted line represents the mean percentage of IFNg^{+} CD8 T cells in the TME of corn oil treated *Ahr*$^{fl/fl}$ *Cd8*-Cre^{-} mice (n = 7 (*Ahr*$^{fl/fl}$ *Cd8*-Cre^{+} corn oil), n = 8 (*Ahr*$^{fl/fl}$ *Cd8*-Cre^{+} I3A), n = 5 (*Ahr*$^{fl/fl}$ *Cd8*-Cre^{-} corn oil), n = 6 (*Ahr*$^{fl/fl}$ *Cd8*-Cre^{-} I3A)). (**f**) B16-F0 tumor growth of mice placed on a low-tryptophan (Trp) diet ((Trp LD), Trp = 0.19%) or high-Trp diet ((Trp HD), Trp = 1.19%) four weeks prior to tumor cell engraftment and orally administered *L. reuteri* or PBS daily starting one day post tumor cell engraftment (n = 8 (Trp LD and PBS), n = 9 (Trp LD and *L. reuteri*), n = 9 (Trp HD and PBS), n = 9 (Trp HD and *L. reuteri*)). (**g**) Tumor weight of mice treated as in (f) on D17 (n = 4 per group). (**h**) Survival analysis of mice treated as in (f) (n = 4 (Trp LD and PBS), n = 5 (Trp LD and *L. reuteri*), n = 5 (Trp HD and PBS), n = 5 (Trp HD and *L. reuteri*)). (**i**) AhR activity measured as luminescence normalized to g tumor derived from luciferase-expressing AhR reporter cells stimulated with tumor homogenate from mice from (f). (**j**) AhR activity from (i) versus tumor weight of mice who were fed a Trp HD. (**k**) B16-F0 tumor growth of mice placed on a Trp LD or Trp HD four weeks prior to tumor cell engraftment and treated IP with aPD-L1 or Iso. ctrl. on D5, 7, 9 and 12 (n = 5 (Trp LD and Iso. ctrl.), n = 4 (Trp LD and aPD-L1), n = 5 (Trp HD and Iso. ctrl.), n = 5 (Trp HD and aPD-L1)). (**l**) Tumor weights of mice from (k) on D14. Data for (a), (c), (f), and (k) represent mean ± SEM analyzed by two-way ANOVA with Sidak's correction for multiple comparisons. Data for (b), (d), and (h) represent comparison of survival curves analyzed by log-rank test. Data for (e), (g), (i), and (l) represent individual mice analyzed by one-way ANOVA with Sidak's correction for multiple comparisons. Mean ± SEM is shown. Data for (j) represents individual mice analyzed by nonparametric Spearman correlation. **P < 0.05, **P < 0.01, ***P < 0.001, ****P < 0.0001*.

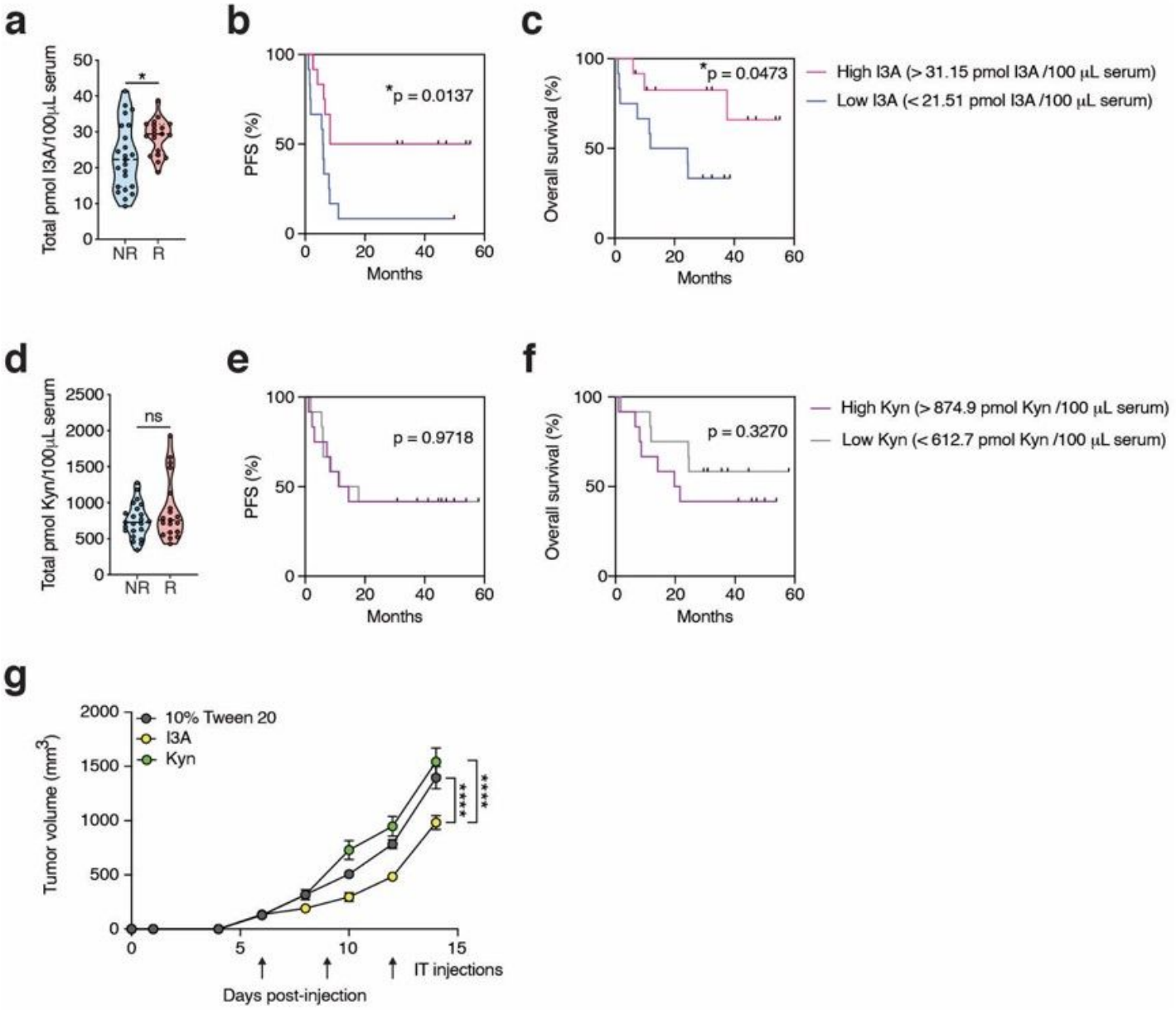

Figure 5

Systemic I3A abundance is significantly increased prior to ICI therapy in advanced melanoma ICI-responsive patients compared to non-responsive patients. (**a**) Quantification of pmol I3A in 100 µl serum of advanced melanoma patients prior to receiving treatment (baseline) with aPD-1 and IFNa (*37*) assessed by mass spectrometry. Samples are grouped by patients' response to ICI therapy. (**b-c**) Kaplan-Meier survival curve comparing progression-free survival (PFS) (b) and overall survival (c) of melanoma patients stratified by pre-treatment I3A sera levels. High I3A [> 70th percentile] with I3A sera levels > 31.15 pmol I3A/100 µL serum (n=12, pink), low I3A [< 30th percentile] with I3A sera levels < 21.51 pmol I3A/100 µL serum (n=12, blue). (**d**) Quantification of pmol Kyn in 100 µl serum of patients from (a) assessed by mass spectrometry. (**e-f**) Kaplan-Meier survival curve comparing PFS (e) and overall survival (f) of melanoma patients stratified by pre-treatment Kyn sera levels. High Kyn [> 70th percentile] with Kyn sera

levels > 874.9 pmol Kyn/100 µL serum (n=12, purple), low Kyn [< 30th percentile] with Kyn sera levels < 612.7 pmol Kyn/100 µL serum (n=12, grey). (**g**) B16-F0 tumor growth of mice IT injected with 200 mg/mL I3A, KYN, or vehicle control (10% Tween 20) every three days starting when tumors reached approximately 150 mm^3 (D6) (n = 5 per group). For (a) and (d) Non-responders (NR) = stable disease or progressive disease, Responders (R) = partial response or complete response (n = 23 (NR), n = 19 (R)). Data for (a) and (d) represent individual patients analyzed by unpaired *t* test. Mean ± SEM is shown. Data for (b), (c), (e), and (f) represent comparison of survival curves analyzed by log-rank test. Data for (g) represents mean ± SEM analyzed by two-way ANOVA with Sidak's correction for multiple comparisons. **P < 0.05*, *****P < 0.0001*; ns, not significant.

Supplementary Files

This is a list of supplementary files associated with this preprint. Click to download.

- SITable1.xlsx
- ExtendedDataTable1.eps
- ExtendedDataFig1.eps
- ExtendedDataFig2.eps
- ExtendedDataFig3.eps
- ExtendedDataFig4.jpg
- ExtendedDataFig5.jpg
- ExtendedDataFig6.eps
- ExtendedDataFig7.eps
- ExtendedDataFig8.eps
- ExtendedDataFig9.eps